ABSTRACT

PHYSICS VALIDATION STUDIES FOR MUON COLLIDER DETECTOR BACKGROUND SIMULATIONS

Aaron Owen Morris, M.S.
Department of Physics
Northern Illinois University, 2011
David Hedin, Director

Muon colliders are under consideration as a possible important future energy-frontier accelerator. A muon collider could be built as a circular accelerator into the TeV energy range as a result of the reduced synchrotron radiation expected from the larger rest mass of muons. Unlike existing lepton (electron/positron) colliders, muons decay with a 2.2 μs lifetime. These decays will produce very energetic electrons off of the beam reference orbit which can generate detector backgrounds that can affect the physics. The main backgrounds include electrons from muon decays, synchrotron radiation from the decay electrons, hadrons produced by photonuclear interactions, coherent and incoherent beam-beam pair-production, and Bethe-Heitler muon production. We will discuss simulation results in terms of observed physics processes in G4beamline.

NORTHERN ILLINOIS UNVIERSITY
DE KALB, ILLINOIS

2011

PHYSICS VALIDATION STUDIES FOR MUON COLLIDER DETECTOR BACKGROUND SIMULATIONS

BY

AARON OWEN MORRIS

A THESIS SUBMITTED TO THE GRADUATE SCHOOL

IN PARTIAL FULFILLMENT OF THE REQUIREMENTS

FOR THE DEGREE

MASTER OF SCIENCE

DEPARTMENT OF PHYSICS

Thesis Director:
David Hedin, Ph.D.

ACKNOWLEDGEMENTS

The author would like to thank the many people who made this research possible. I would especially like to thank my advisor, David Hedin, for getting me on this project. Likewise, I would like to thank my collaborators Steve Kahn, Mary Anne Cummings, and Tom Roberts at Muons, Inc. and Joseph Kozminski at Lewis University and Chason Zacher at NIU. Without them, my progress would have stalled out long ago.

I would also like to extend my gratitude and thanks to the entire staff of Muons, Inc., including Rolland Johnson, Chuck Ankenbrandt, Bob Abrams, Cary Yoshikawa, Kevin Beard, Gene Flanagan, and Jim Nipper.

I would like to thank the Muon Accelerator Program, specifically Estia Eichten, Steve Geer, and Nikolai Mohkov.

Furthermore, I would like to thank Suzanne Willis for being on my thesis committee along with my direct collaborators, David Hedin and Mary Anne Cummings.

I would like to also extend my gratitude to the other members of the Department of Physics, especially my professors and my fellow graduate students.

And, of course, I would like to thank my family.

DEDICATION

“For the future.”

TABLE OF CONTENTS

LIST OF TABLES

LIST OF FIGURES

Page

LIST OF APPENDICES

This list is a placeholder version in this draft.

CHAPTER 1:

INTRODUCTION

"Never fear answers, only fear running out of questions."

Commander Susan Ivanova, Babylon 5

Within the broad discipline of physics, the study of the fundamental forces of nature and the most basic constituents of the universe belongs to the field of particle physics. While frequently referred to as "high-energy physics," or by the acronym "HEP," particle physics is not driven just by the quest for ever-greater energies in particle accelerators. Rather, particle physics is seen as having three distinct areas of focus: the cosmic, intensity, and energy frontiers. These three frontiers all provide different, but complementary, views of the basic building blocks of the universe.

Currently, the energy frontier is the realm of hadron colliders like the Tevatron at Fermi National Accelerator Laboratory (Fermilab) or the Large Hadron Collider (LHC) at CERN. While the LHC is expected to be adequate for explorations up to 14 TeV for the next decade, the long development lead time for modern colliders necessitates research and development efforts in the present for the next generation of colliders. This paper focuses on one such next-generation machine: a muon collider. Specifically, this paper focuses on Monte Carlo simulations of beam-induced backgrounds vis-à-vis detector region contamination.

Subsequent chapters are structured to begin with a general introduction to particle physics and accelerators before addressing the specifics of a muon collider. This thesis

then discusses the Monte Carlo simulations in specific regard to the verification of the physics program G4beamline.

For purposes of consistency, all particle and material properties are derived from the Particle Data Group and are listed in the appendices. Likewise, acronyms and abbreviations are listed in Appendix C.

This research was made supported by DOE STTR Grant DE-SC00005447 and the Department of Physics at Northern Illinois University. Portions of this thesis were presented at the Workshop on Detector R&D (October 7-9, 2010 at Fermilab) and the Particle Accelerator Conference (PAC) 2011 (March 28-April 2, 2011 in New York City). Additionally, preliminary results and conclusions were presented at PAC. (Morris *et al*. 2011, Kahn *et al*. 2011)

CHAPTER 2:

INTRODUCTION TO PARTICLE PHYSICS

"Then I will tell you a great secret, Captain. Perhaps the greatest of all time. The molecules of your body are the same molecules that make up this station, and the nebula outside, that burn inside the stars themselves. We are star stuff. We are the universe made manifest, trying to figure itself out. And as we have both learned, sometimes the universe requires a change of perspective."

Ambassador Delenn, Babylon 5

2.1 Introduction

Until recently, the Tevatron at Fermilab was the highest-energy particle accelerator in the world, with proton-antiproton $(p\bar{p})$ collisions with a center-of-mass energy $(\sqrt{s})$ of 1.96 TeV. The LHC at CERN now holds the record with $\sqrt{s} = 7\ TeV$ for proton-proton (pp) collisions and has plans to increase to $\sqrt{s} = 14\ TeV$.

In order to reach ever higher energies, particle accelerators must increase in size due to technological limitations in terms of beam control and acceleration. Additionally, despite the 350% increase in energy between the Tevatron and the LHC, only fractions of that energy enter into collisions through parton-parton interactions. Partons, of course, are the point-like constituents of composite particles.

Protons (or antiprotons in the Tevatron) are composite subatomic particles. Each proton (antiproton) contains three quarks (anti-quarks) bound together by gluons, specifically two up (u) quarks and a down (d) quark (or two anti-ups $(\bar{u})$ and an anti-down $(\bar{d})$). The rest mass of a proton is 938.3 $\frac{MeV}{c^2}$; whereas the masses of the up and down quarks are about 2.5 $\frac{MeV}{c^2}$ and 5.0 $\frac{MeV}{c^2}$, respectively. As such, the overwhelming majority of mass-energy of a proton results from strong interactions between the valence quarks, specifically the mechanism of chiral symmetry breaking. (Martin 2011) This makes event reconstruction difficult as you must determine which initial partons (*i.e.* valence or sea quarks, gluons) actually collided. In contrast, the most obvious simplification is to collide point-like particles (*e.g.* electrons), rather than composite ones (*e.g.* protons, antiprotons). However, the energy frontier has long generally been the realm of hadron colliders like the Tevatron or LHC, as demonstrated in Figure 1. The largest lepton collider, the Large Electron-Positron (LEP) collider, also at CERN, achieved $\sqrt{s} = 209\ GeV$ before its dismantling in 2000. However, LEP was designed as a precision instrument, first as a Z^0 factory and then as a W^+W^- factory.

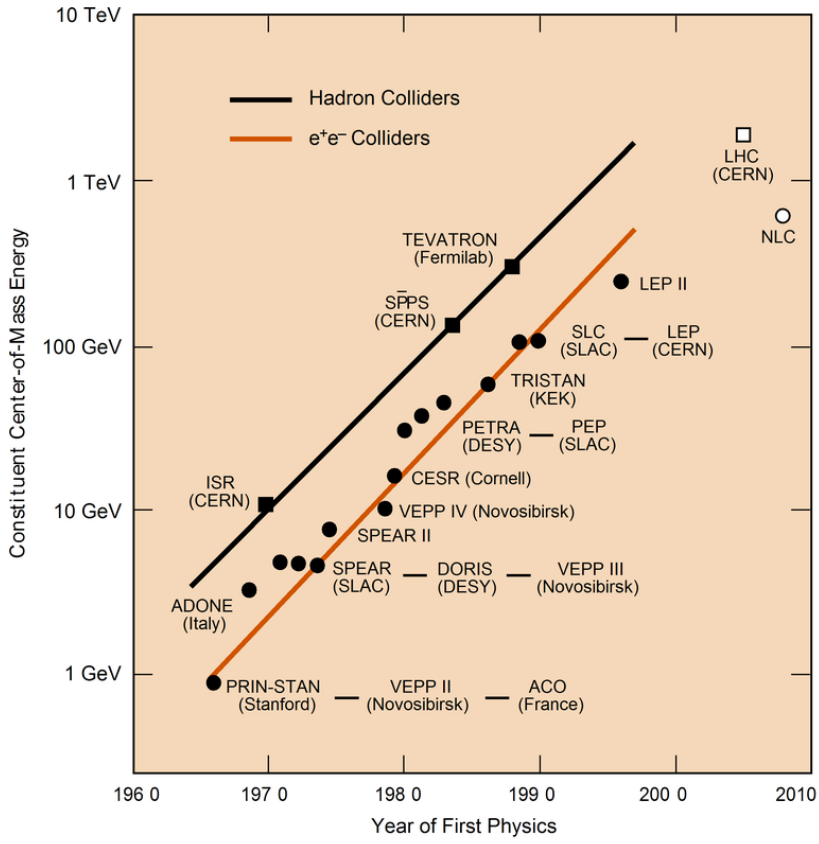

Figure 1: Livingston plot.
This figure compares hadron and e^+/e^- colliders based on constituent center-of mass energy (hence why the Tevatron is below 1.96 TeV). (Panofsky 1997)

2.2 The Standard Model

The Standard Model (henceforth, SM) is the currently accepted theory linking electromagnetism, the weak force, and the strong nuclear force to each other and to the known fundamental particles. There is one additional fundamental force, gravity, but there is no quantum mechanical description of it within the SM, though supersymmetric (SUSY) theories incorporate it.

Within the SM there are twelve fundamental particles and four force-carrying (gauge) bosons. The twelve fundamental particles are considered point-like and, therefore, non-composite under the SM. They all obey Fermi-Dirac statistics and are thus known as the fundamental fermions. Additionally, it should be noted that all twelve of these fundamental fermions have antiparticles.

The fundamental fermions are divided into two types. Six of the fundamental fermions are quarks, which experience all four fundamental forces, and the other six are leptons, which do not experience the strong nuclear force. Quarks experience the strong nuclear force (and leptons do not) and so we assign quarks a quantum number called "color" (and do not assign color to leptons). The three colors, called red, green, and blue, are never observed as all quarks form colorless bound states and are thus never found as free particles. There is no difference between different colors of quarks as they are perfectly degenerate with each other. Those bound states are called hadrons, which come in two subtypes: quark-antiquark $(q\bar{q})$ pairs known as mesons and three quark groupings known as baryons. The exception to the bound state rule is the top quark, which decays before it can form any bound state.

The remaining six fermions, the leptons, contain two separate subclasses: the neutrinos and their charged counterparts. All leptons interact through the weak force and gravity. The three neutrinos $(\nu_e, \nu_\mu, \nu_\tau)$, with masses likely on the order of eV or less and carrying no charge, interact neither electromagnetically (being electrically neutral) nor strongly (being leptons). The remaining three "down-type" leptons, the electron (e), muon (μ), and tau (τ), interact electromagnetically (having charge -1) but not strongly.

The fundamental fermions can be grouped into three generations with each subsequent generation being a heavier version of the previous, as shown in Figure 2 below. Within each generation, the fermions can also be organized as "up-type" or "down-type," which merely represent their matrix form in quantum field theory calculations.

The four force-carrying bosons, the photon, gluon, Z^0, and $W^{\pm}$, moderate the interactions between the fermions. The photon moderates the electromagnetic interaction, the gluon moderates strong nuclear interactions, and the Z^0 and $W^{\pm}$ bosons moderate weak force interactions.

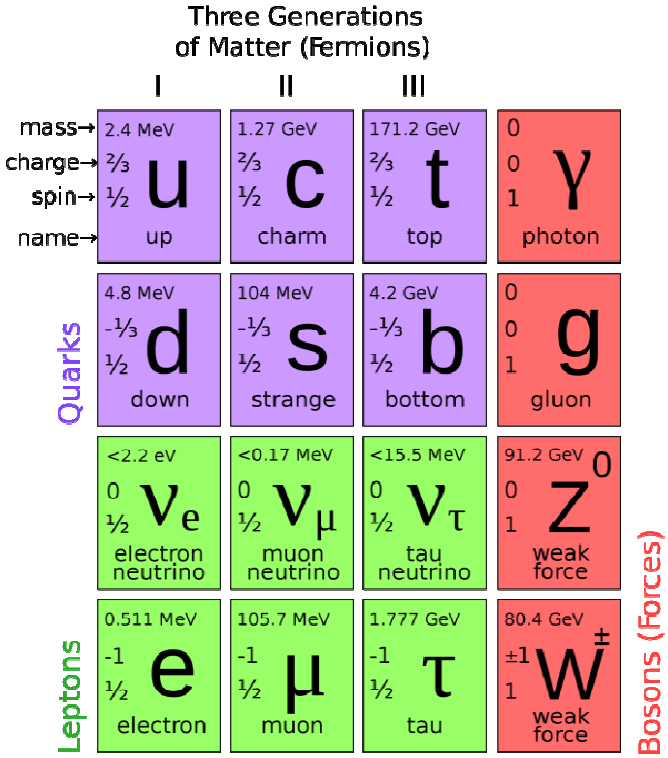

Figure 2: The Standard Model.
A common, concise variant of the Standard Model diagram organized horizontally by generation (first three columns) and vertically analogously to matrix form representation. The fourth column is a list of the gauge bosons. Mass (approximate), charge, and spin values are also provided. (Wikipedia 2006)

2.3 Lepton Colliders

Up until now, all purely lepton colliders have been electron-positron (e^-e^+) colliders. However these colliders have physical limitations as a consequence of the small mass of the electron $\left(0.511\ \frac{MeV}{c^2}\right)$. Any charged object, such as an electron or a proton, that undergoes an acceleration radiates energy. Per introductory classical mechanics, acceleration can be characterized either by a change in linear velocity or by a change in trajectory at constant velocity. As a result, it is impossible to accelerate any charged object without some loss of energy.

For a change in trajectory, as is required for circular accelerators like LEP, electrons radiate more energy away as their paths get bent than they will gain in accelerating elements. The aforementioned LEP represents the practical engineering limitation to electron (positron) circular machines. However, some accelerators take advantage of this synchrotron emission as a means to produce well-characterized intense photon beams (such as the Advanced Photon Source at Argonne National Laboratory or the National Synchrotron Light Sources at Brookhaven National Laboratory), but in terms of reaching the energy frontier, circular electron/positron accelerators become economically and technologically infeasible.

Linear accelerators (linacs) are an alternative and there are two plans for a next-generation energy frontier accelerator: the International Linear Collider (ILC) and the Compact Linear Collider (CLIC). In the case of linear acceleration, radiative losses do not become significant until the energy gain is of the order of $200\ \frac{EeV}{m}$, which is $\gtrsim 10^{12}$ times currently realized [linear] accelerating gradients. (Jackson 1999) Though

technologically feasible, unlike in storage ring or recirculating accelerators, the beam will only see each component of the accelerator once. This introduces a variety of logistical and control challenges that are outside the scope of this paper.

The other alternative is to use a higher mass lepton, such as the muon, in a circular accelerator. Muons have masses of $105.7\ \frac{MeV}{c^2}$, which is over 206 times the mass of the electron. Radiative losses due to synchrotron emission scale as the inverse square of the masses, meaning that muons radiate over 42,000 times less than electrons (but only 79 times more than protons). Unfortunately, muons decay with a lifetime of $2.2\ \mu s$.

Notably, with the reduced radiative losses inherent in circular muon accelerators, it is possible to build a muon collider significantly smaller than LEP. In fact, the Muon Accelerator Program (MAP), is promoting the idea that a muon collider could be built entirely on the Fermilab site, unlike any of the alternative next-generation colliders. Figure 3 demonstrates the differences in scales between the four leading next-generation plans (muon collider, ILC, CLIC, VLHC), Fermilab, and the Chicago metropolitan area. It should be noted that not all of these colliders are proposed to be built at or near Fermilab, or even domestically within the United States.

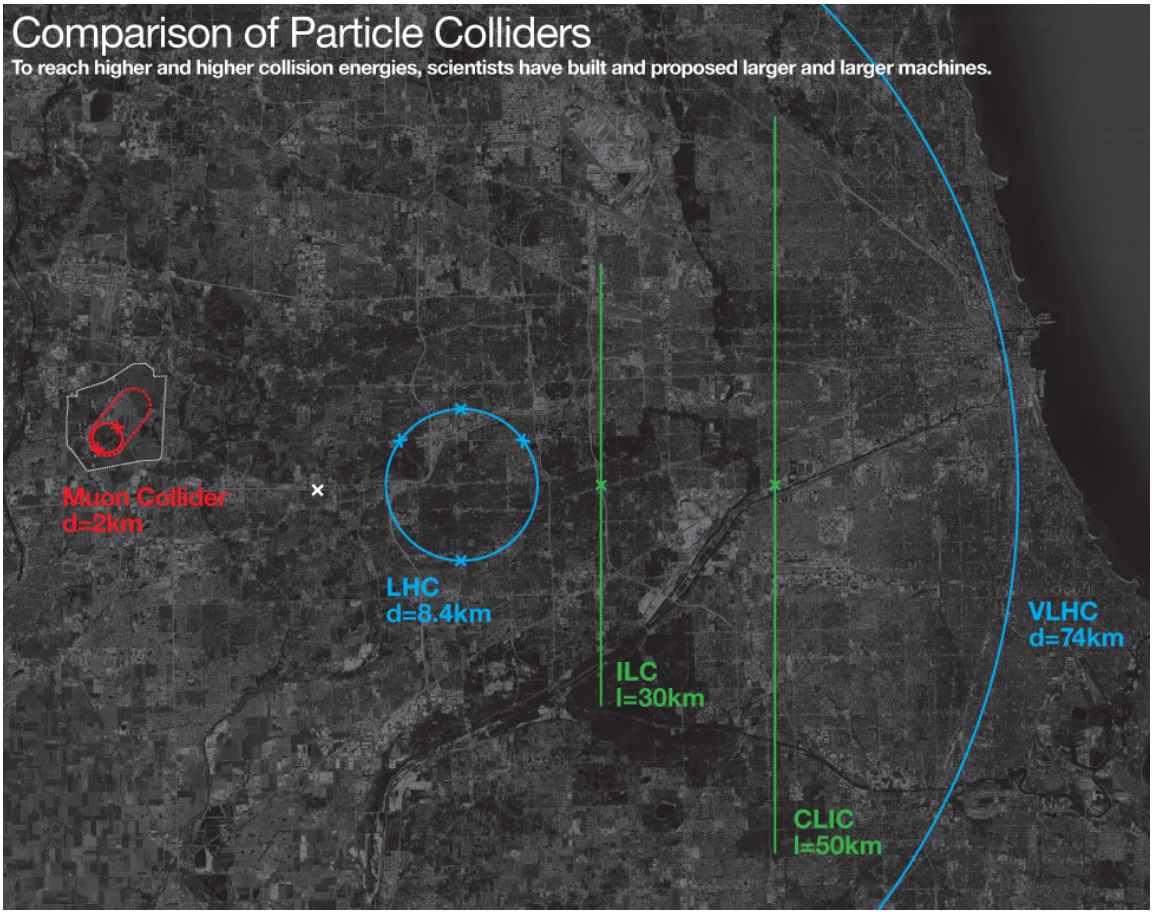

Figure 3: A comparison of current and future colliders with the Chicagoland area. Four possible future colliders and the LHC are overlaid on the Chicago metropolitan area with the Fermilab site indicated. Only the muon collider is proposed to be built at Fermilab. North is up. (MAP 2010)

If a muon collider were to be constructed at Fermilab, the actual colliding ring would fit inside the current Tevatron ring, though there would be production and accelerating components located elsewhere on the site. Figure 4 is a schematic layout of such a conceptual design, including multiple accelerating stages.

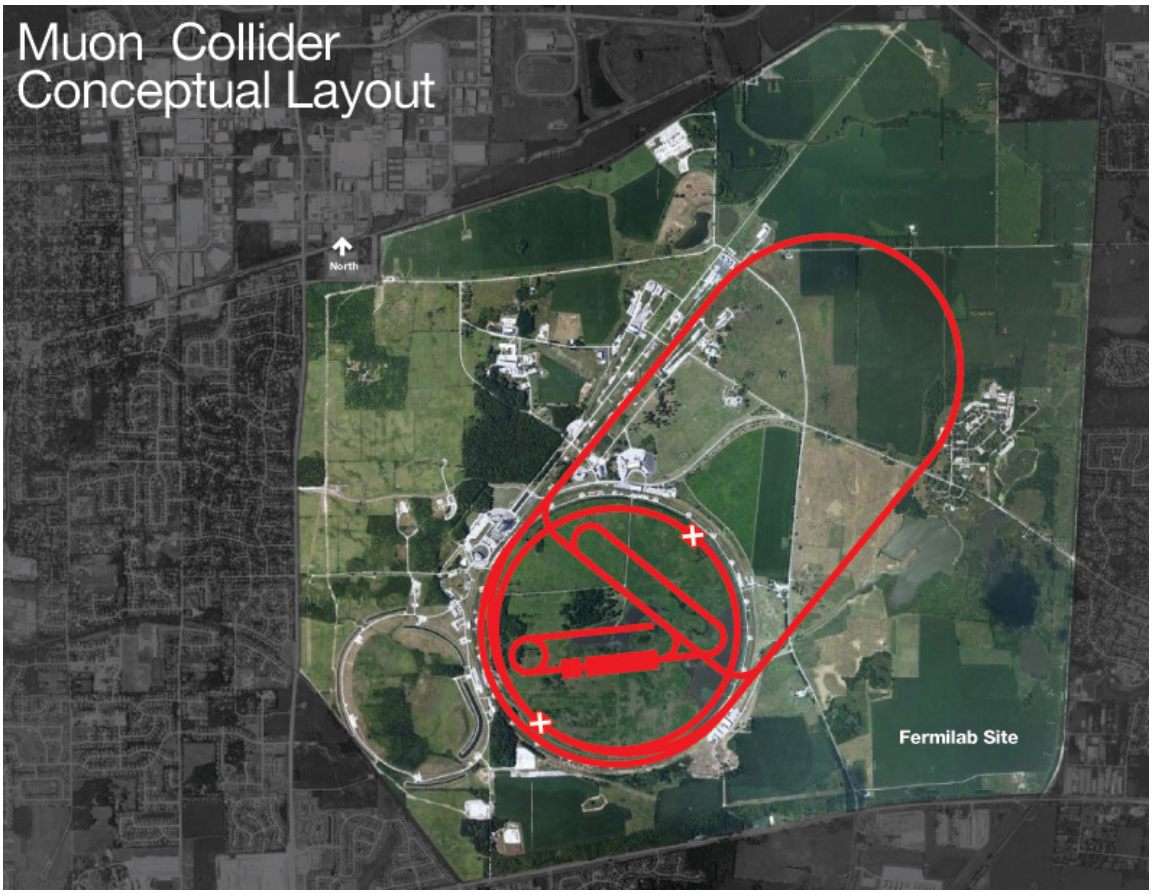

Figure 4: A conceptual illustration of a muon collider at Fermilab.
This aerial view of the current Fermilab site with a conceptual design of a muon collider overlaid to demonstrate relative size with respect to both the Tevatron and the site itself. North is up. (MAP 2010)

2.4 Muon Decay

Muon decay is almost always a three-body decay with the muon decaying into two neutrinos and an electron. Tree-level decays, known also as Michel decays, are exactly three body decays where $\mu^- \rightarrow \nu_\mu \overline{\nu_e} e^-$ or $\mu^+ \rightarrow \overline{\nu_\mu} \nu_e e^+$ with a $W^\mp$ propagator allowing for conservation of charge and lepton family number (muon and electron

numbers). There is only one tree-level Feynman diagram for Michel decays, shown in Figure 5.

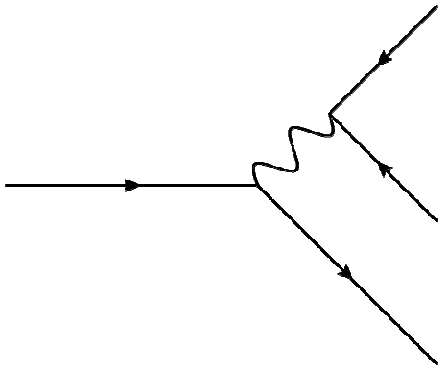

Figure 5: Feynman diagram for Michel decay.

In the center-of-momentum frame, the only preferred direction for the outgoing electron to be emitted is along the muon spin polarization direction. For an ensemble of muons, this will average out such that the decay electrons have a defined range of energies as a result of recoils against the neutrinos. At tree-level in the center-of-momentum frame, the decay electron can have —. Boosting these decays along a beam reference orbit will produce a Michel distribution such as the one in Figure 6.

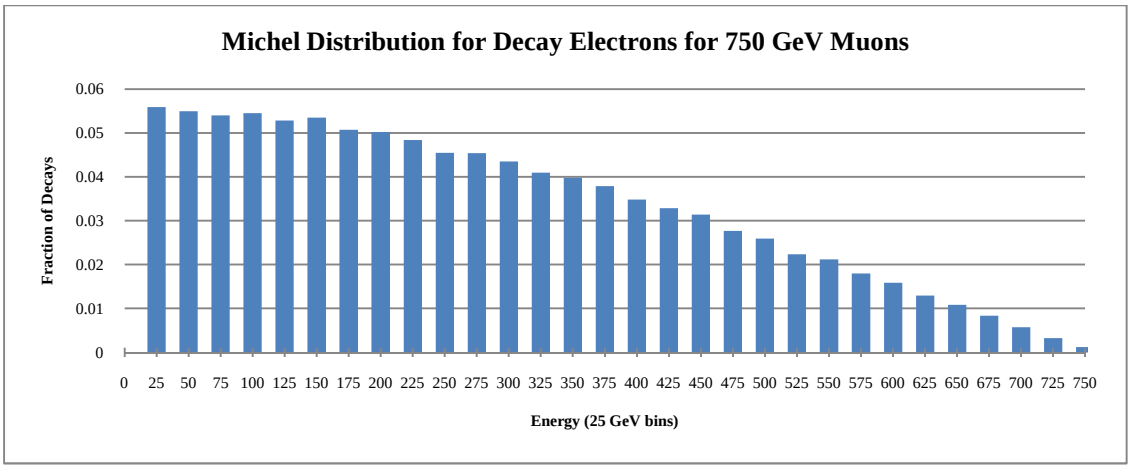

Figure 6: Sample Michel distribution.
The above distribution shows the fraction of decay electrons in a given 25-GeV bin for a 750 GeV muon beam.

The first-order radiative corrections to muon decay, $\mu^- \rightarrow \nu_\mu \overline{\nu_e} e^- \gamma$ or $\mu^+ \rightarrow \overline{\nu_\mu} \nu_e e^+ \gamma$, have branching rations of the order of 0.01%. Other decay modes, including possible lepton family number violating decays, have maximum branching rations of similar order or smaller. We can therefore assume that muon decay is entirely a tree-level process in terms of its background contribution.

CHAPTER 3:

MUON COLLIDERS

"Modern technology makes anything possible."

Sarge, Red vs. Blue

The concept for a muon collider dates back to 1969 with Gersh Itskovich Budker. (Cline 1996). Budker's idea was to use "mu mesons," as muons were known at that time, to reach $\sqrt{s}$ of a few hundred GeV. The concept continued to be developed over the following decades with Neuffer suggesting a Z^0 factory with colliding muon beams in 1979 (Neuffer 1979) and Skrinsky suggesting the feasibility of a muon collider in 1980. (Skrinsky 1980). While such low-energy ranges are now ideal for precision physics, most current plans call for $\sqrt{s}$ to be on the order of TeV. These energies are required to probe beyond the Standard Model (BSM). (Ankenbrandt *et al*. 2008)

Starting in the mid-1990s, plans for muon colliders began to narrow down to the range of $0.1\,TeV \leq \sqrt{s} \leq 4\,TeV$ (50×50 GeV through 2×2 TeV). (Geer 2009) The lowest energy colliders would be [Standard Model] Higgs factories, designed to perform precision measurements such as those performed at B factories (*e.g.* BaBar at SLAC) or at $Z^0/W^{\pm}$ factories (*e.g.* LEP at CERN). Higher energy colliders would, of course, be energy frontier machines designed to probe the BSM region.

The muon mass implies that only high-energy natural processes can create them. The main natural source of muons is from secondary cosmic ray showers. The bulk of the atmosphere is opaque to cosmic rays and thus the primary cosmic rays (typically

protons or other light ions) will interact with atmospheric nuclei (*e.g.* nitrogen, oxygen) and form a shower of secondary cosmic rays. Pions are preferentially created in primary cosmic ray interactions. If the pion is charged, it decays into muons (which decay into electrons and neutrinos) and neutrinos. Neutral pions, of course, decay into gamma ray pairs. The gamma rays, provided they are of sufficient energy, can cause e^-e^+ pair production or even $\mu^-\mu^+$ pair production. The electrons, being low-mass charged particles, will electromagnetically interact with other particles in the atmosphere, which causes further emission of gamma rays (bremsstrahlung radiation), which in turn can create more lepton pairs. Indeed, it is from such cosmic ray showers that the muon was first discovered. (Bradt 2004)

In a muon collider, muons will be created through the same set of processes as in a cosmic ray shower. Current plans call for a multi-megawatt GeV-scale proton driver (such as Project X at Fermilab) to collide protons with some sort of pion production target (such as a flowing liquid mercury target (*e.g.* the Mercury Intense Target (MerIT)). This "front-end" of a muon collider would be embedded within a magnetic field to maximize $\pi^{\pm}$ capture and containment during their decays prior to further cooling and acceleration of the decay muons. In between the front-end production and the accelerator/collider complex would be a six-dimensional cooling mechanism (or set of mechanisms). These pre-acceleration components of a muon collider are illustrated in Figure 7.

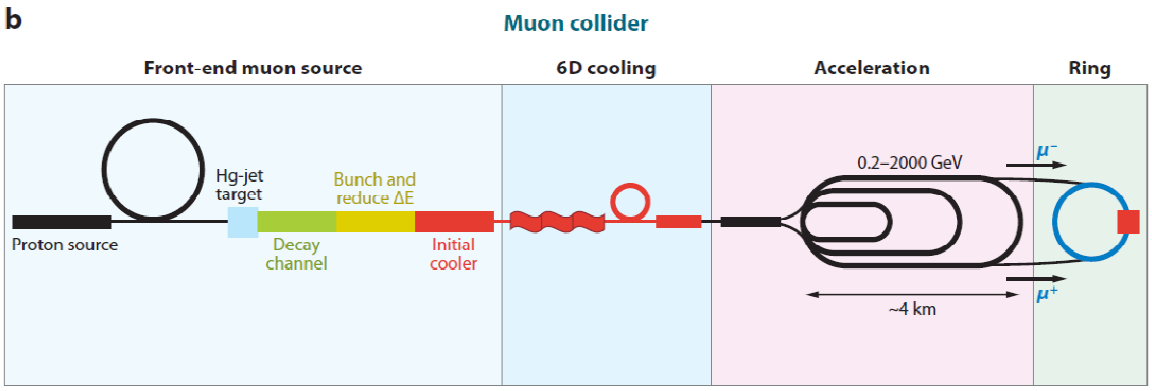

Figure 7: Schematic of a muon collider.
The above schematic isolates the main components of a muon collider into four regions (front-end, six -dimensional cooling, acceleration, and collider). (Geer 2009)

Cooling refers to the reduction in six-dimensional (6D) phase space (the spatial dimensions (x, y, z), and the momenta (p_x, p_y, p_z)) to ensure the particle beam (or bunch) can fit inside the beampipe and is within the acceptance of an accelerating radio frequency (RF) cavity. In general, muon cooling schemes involve ionization cooling in high-pressure, hydrogen-filled RF cavities (HPRF). The specifics of both the pion/muon production and muon cooling are outside the scope of this paper.

These muons will then undergo acceleration in a recirculating linac ("racetrack") accelerator before being sent into a collider/storage ring. The effects of ultra-relativistic time dilation on these muons will increase their lab-frame lifetimes such that it is possible to accelerate and collide them, though some fraction will still decay in-flight.

MAP suggests that the possible layout of a muon collider, Figure 8, would be based around Project X but would also allow for a neutrino factory (or factories) and other precision experiments.

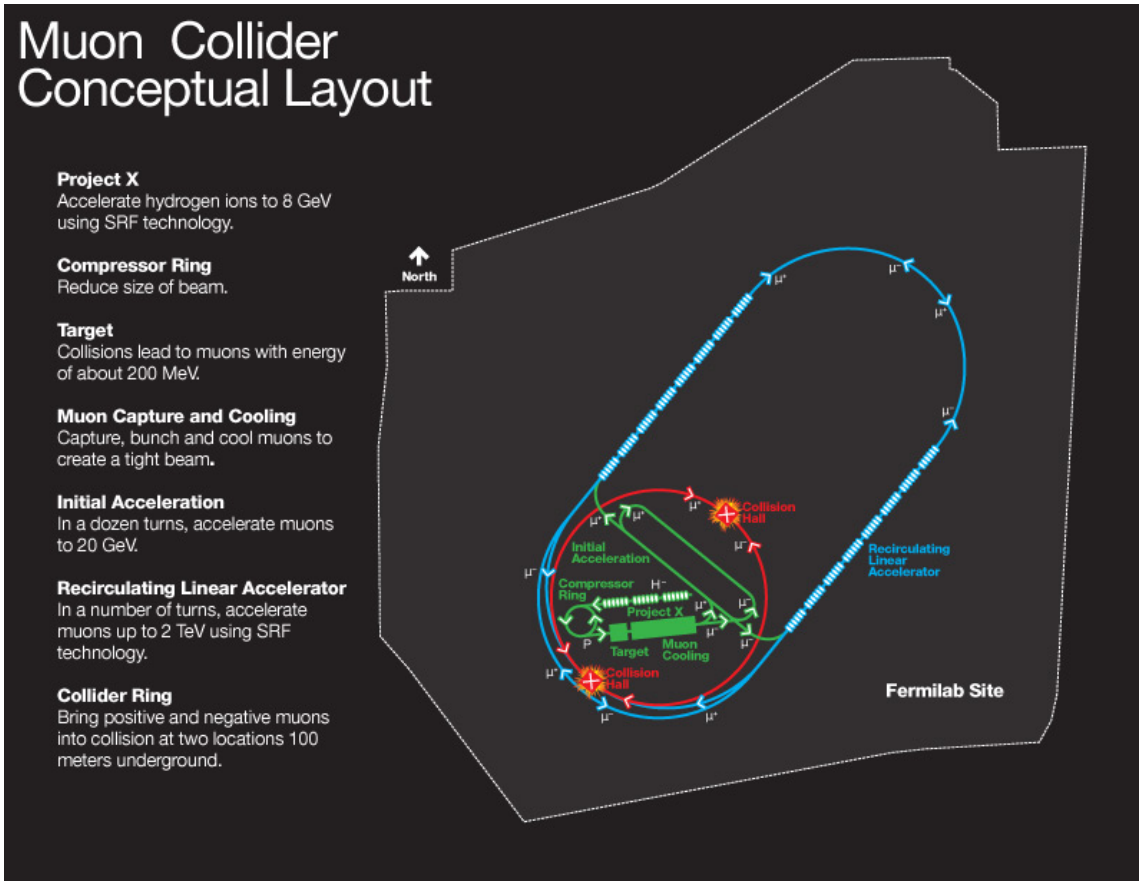

Figure 8: A detailed schematic of a possible muon collider facility at Fermilab. The figure above is a detailed version of the muon collider seen in Figure 3 and Figure 4 with Project X as a proton driver. (MAP 2010)

The detector region itself will be characterized by large shielding cones, designed to reduce muon decay products from reaching the active detector volume. While all detectors at particle colliders have some region around the interaction point that cannot be instrumented (*e.g.* the beampipe itself) or is too active for good resolution (*e.g.* near the beampipe), a muon collider will have up to 0.76 steradian (6%) taken up by a shielding cone around the beampipe.

As seen in Figure 9, it was originally assumed that a 20° cone would be sufficient to reduce the background within the detector volume to be comparable to the background

at the LHC. More recently, however, it is being investigated whether the cone can be reduced to as low as 6° without impacting the physics capability of a detector. (Kahn *et al*. 2011) In the event that a larger angle is required, it is likely that the shielding cone will be at least partially instrumented in order to recover some physics ability.

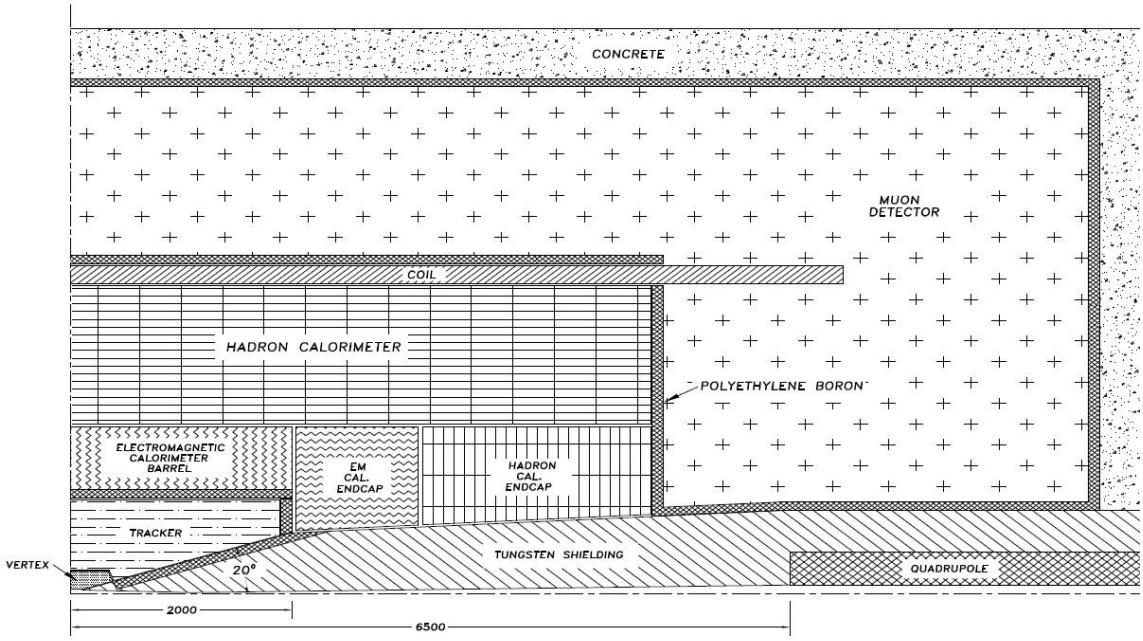

Figure 9: Cutout of a generic detector layout at a muon collider.
This quadrant of a generic detector volume features a 20° shielding cone though the vertex tracking region. (Palmer *et al*. 1996)

Along the beamline, there are various designs to attempt to eliminate line-of-sight routes between interior surfaces and the detector volume. This is to avoid particles from showers from halo impacts from breaching the detector volumes. These designs range from having a sawtoothed interior within the cone (Figure 10) to nozzle-like designs.

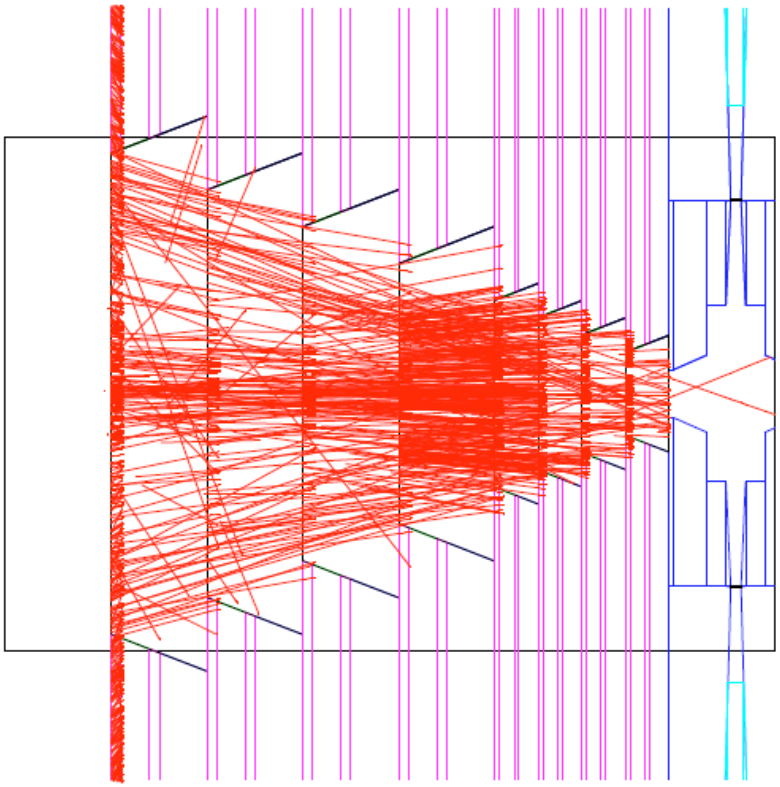

Figure 10: Shielding cone with sawtooth interior.
A schematic of the interior of a shielding cone with a sawtooth pattern. Red lines are sample muon decay tracks. (Palmer *et al*. 1996)

One alternative to a pure cone is a bent cone, which could reduce the impact on the detector volume. In the nozzle design used by our research group, the outer cone changes angle at different distances from the interaction point following the example in Figure 11. Additionally, at distances greater than 1.05 meters, there is a cladding of borated polyethylene as a neutron shield.

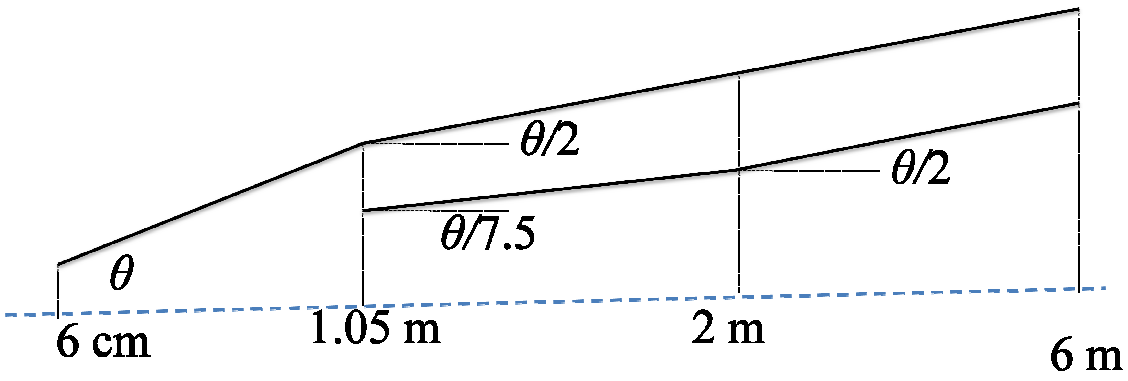

Figure 11: Schematic of varying cone angles.
A schematic of how the outer cone angle varies as a function of distance from the IP.

As such, the beamline shielding in the detector volume takes the form of Figure 12, where sample tracking planes are shown immediately around the interaction point.

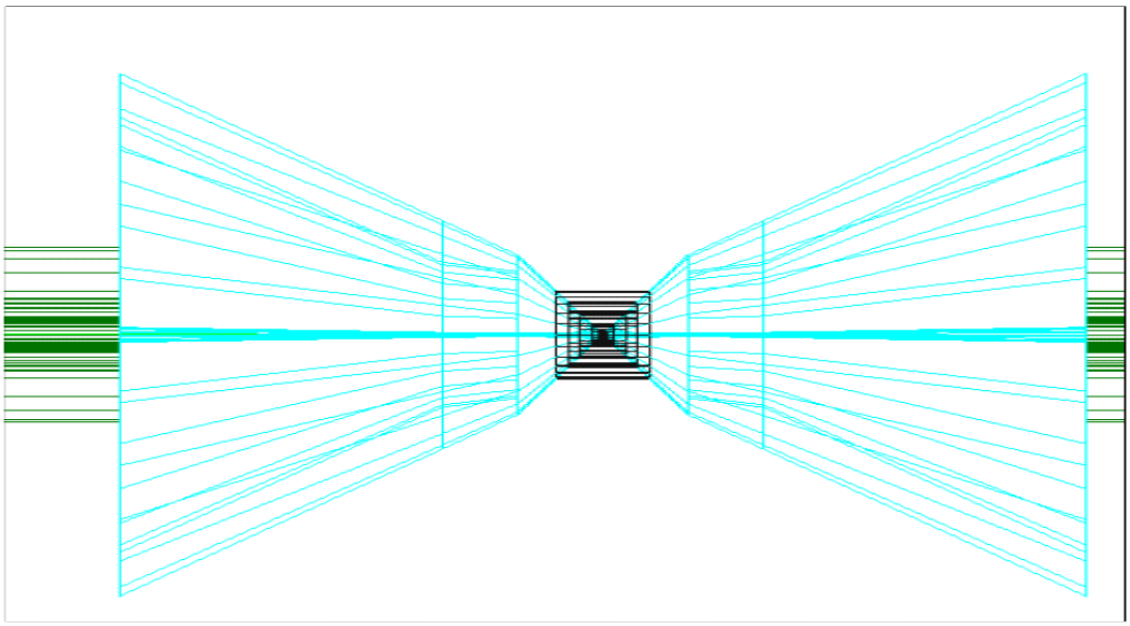

Figure 12: Schematic of the conical shielding in the detector volume.

CHAPTER 4:

BACKGROUND STUDIES

"Skepticism is the language of the mind."

Lorien, Babylon 5

One of the consequences of the finite muon lifetime is the production of backgrounds that could potentially "spoof" physics events in the detector volume of a muon collider or cause radiation damage to the collider or detector. The majority of background events, produced from muon decays or other interactions, will occur far from the detector volumes and thus distance (and all intervening materials) will be the main source of shielding for the detector. However, any backgrounds produced within ±150 meters of the interaction point (defined as the predetermined position in the center of the detector volume where the beams of muons and of antimuons are collided) have a far greater chance of affecting the physics analysis within the detector.

The main background sources result from muon decays which produce very energetic off-axis electrons. These decay electrons will emit high-energy photons (through synchrotron and bremsstrahlung), which in turn can create hadrons through photonuclear interactions. Additionally, photonuclear interactions can result in Bethe-Heitler muon pair production, which could readily enter any detector volume and mimic physics events.

As Figure 7 implies, the layout of a muon collider is still in flux. The main determinants are LHC results, specifically at which energies (if at all) new physics

(particles) are found. As such, there are plans ranging from $50 \times 50\, GeV$ to $4 \times 4\, TeV$ μ^+/μ^- beams at various bunch configurations. For the purposes of this study, we assume $\sqrt{s} = 1.5\, TeV$ via $750 \times 750\, GeV$ μ^+/μ^- beams with 10^{12} μ per bunch. Such a setup produces 4.3×10^5 muon decays per meter per beam. While this specifies certain limits for simulation parameters (see the above Michel distribution in Figure 6), it does not change which background processes occur, just their respective rates and energies.

As stated previously, the vast majority of decay products will not affect the detector region at all as they will be produced sufficiently downstream that they will interact long before they reach the interaction region. Decay products with near-line-of-sight access to the interaction region are likely to be from within ±150 meters. In our studies of detector backgrounds, the focus is on a collider lattice which is ±75 meters from the interaction region, as shown below in Figure 13.

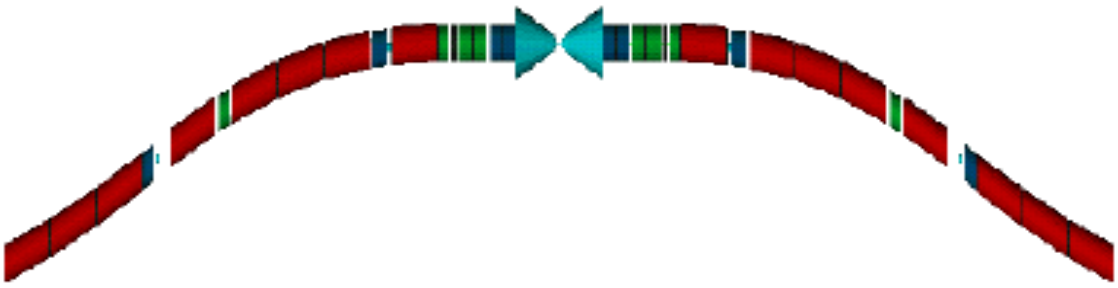

Figure 13: ±75 m from the IP of a muon collider lattice.

The above figure features a 10° tungsten shielding cone (shown in teal) in addition to the magnet elements within ±75 m. The scale is 10:1 x:y. (Gianfelice-Wendt 2010)

3.1 G4beamline

There are a few main simulation suites used for muon collider studies. One is MARS, a Monte Carlo code which can simulate a variety of hadronic and electromagnetic showers including thermal neutron and low-energy photon content. (Mohkov 2010) MARS, generally speaking, is used for its ability to determine radiation dosage, but is also capable of single-particle tracking. Another multi-particle tracking suite is FLUKA, which has been generalized for multipurpose use from a high-energy radiation shielding program. (Fasso *et al*. 2011)

The majority of single-particle tracking simulations are through the simulation suite, GEANT4. GEANT4 is a highly flexible program designed for single particle tracking, but it requires significant foreknowledge of computer programming, including the object-oriented C++ language. (GEANT4 2011)

As such, within GEANT4, the complexity of the simulation code can be higher than the complexity of the simulation itself. We bypass this problem by using an overlay for GEANT4, G4beamline, as our interface to the simulation software.

G4beamline, specifically designed for simulating beamlines, is a single particle tracking and simulation program built on top of GEANT4 as both a graphical user interface (GUI) and as a command-line interface. (Roberts 2011) The main advantage of G4beamline is that the simulation description is of the same order of complexity as the system that is itself being simulated. Thus, users without C++ coding experience can rapidly begin constructing simulations that meet their needs with built-in beamline elements.

G4beamline is available as a single executable for most modern computing platforms (*e.g.* Windows, Linux) so most users will not need to build G4beamline, GEANT4, nor any of their associated libraries. It is still possible, of course, to install secondary GEANT4 data files such as thermal neutron cross sections. Source files for G4beamline are also available for users who wish to add their own customized beamline elements, though this does require some C++ coding.

A G4beamline input file is a single ASCII file containing the geometric, material, and field parameters for the beamline elements. These inputs can also include variations to global simulation parameters if required.

The output format is customizable, but for the purposes of this study we use "virtual detectors" within and around simple targets to output ROOT NTuples that track any particle passing through the virtual detector's volume. These outputs have the units of millimeters (position), MeV/c (3-momentum), nanoseconds (time), and standard Particle Data Group particle ID. It should be noted that a virtual detector, by definition, takes on the material properties of its enclosure and will record secondaries produced within its volume once they take a step. (Roberts 2011)

For purposes of this study, we used two main physics engines: QGSP_BERT and QGSP_BERT_HP. These engines are both based on the quark-gluon-string (QGS) model with a precompound nucleus model in addition to a few LEP models and the standard electromagnetic package. (Wright *et al.* 2006) Additionally, both physics lists use BERT, which is the GEANT4 Bertini cascade for primary hadrons below ~10 GeV, which yields better comparisons to experimental data than the LEP models. (GEANT4 2011) The _HP, or "High Precision," engine uses the high precision neutron package

(NeutronHP) to transport neutrons down to thermal energies. The use of QGSP_BERT_HP requires the installation of the G4NDL.3.14 dataset, available at the GEANT4 downloads page. (GEANT4 2011)

3.2 Simulation Studies

Beamline muon decays will produce electrons (and neutrinos). Those electrons will have energies described by a boosted Michel distribution (Figure 6) and those electrons will produce high-energy photons through synchrotron emission and bremsstrahlung. Both these electrons and photons will proceed to interact with collimating masks, magnet elements, and detector shielding to produce secondary electromagnetic showers. Studies of these electromagnetic showers are discussed first.

Photonuclear neutron production will also be carefully examined as these neutrons will survive multiple beam crossings and will contribute heavily to the background in hadronic calorimeters, and to possible radiation damage of detector and accelerator elements. The simulation of neutron-absorbing materials, such as borated polyethylene will be considered. Finally, photonuclear pair production of muons (Bethe-Heitler production) is discussed.

In general for these physics validation studies, single particle beams at a single energy with no transverse momentum are generated incident on solid cylinders of material (*e.g.* tungsten, iron) with no magnetic or electric fields present. This simplification allows for similar processes to be disentangled from each other, thus allowing individual physics processes to be confirmed as present. The G4beamline

simulation results are compared with calculated theoretical results in order to ensure that the physics processes are working properly. This work therefore contributes to G4beamline validation documentation.

3.3 Electromagnetic Showers

In the current design for a muon collider, a series of tungsten collimating masks are placed between magnet elements to strip off the beam halo. The beam halo is comprised of muons which are offset from the reference orbit(s) as well as any decay or interaction secondaries that are traveling with the beam. Direction simulations of muon beams halos are infeasible at this stage, mainly due to computational limits resulting from the relatively long muon lifetime and the large bunch sizes. That said, simulations of the halo are ongoing via use of the Michel decay spectra through a reference lattice provided by Gianfelice-Wendt. For purposes of physics validation, we are not simulating even this refined halo, but rather so-called “clean” beams which are directly incident on [fundamental] targets with simple geometries (cylinders). An example of one of these showers is shown below in Figure 14.

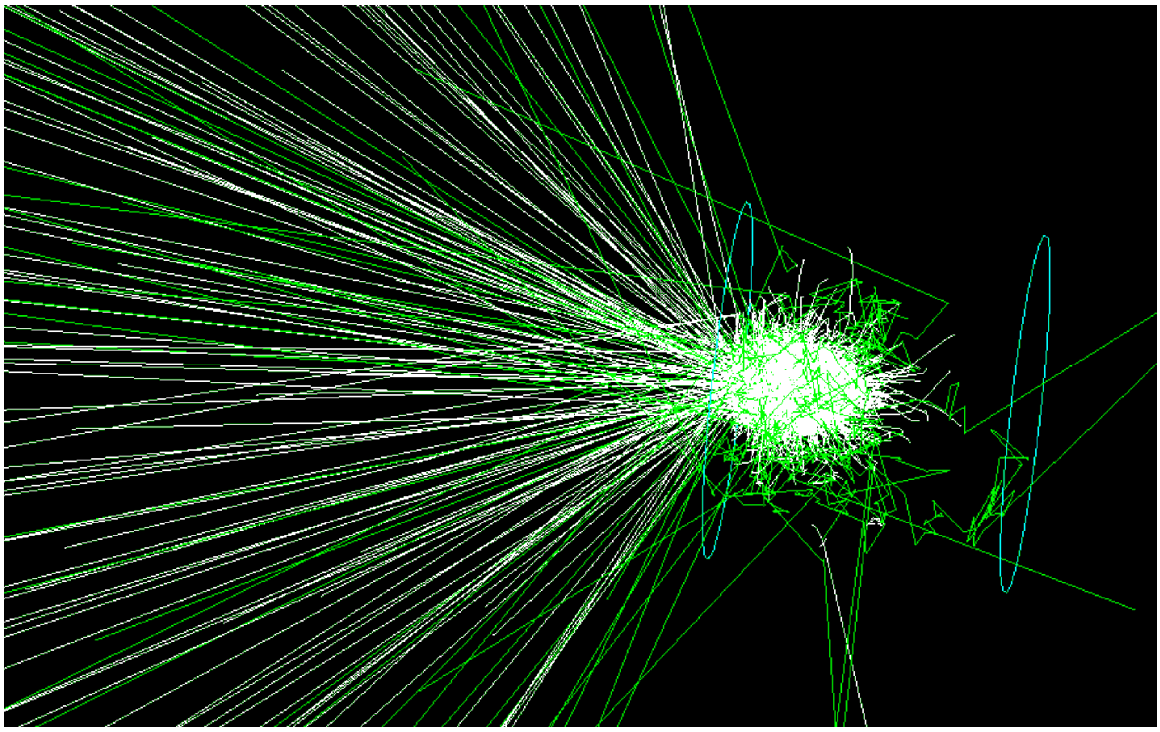

Figure 14: A visualization of a single GeV-scale electromagnetic shower. This visualization is for a single GeV-scale electron impacting on a tungsten cylinder from the left. The endcaps of the target are defined by teal discs. The white tracks are photons and the green tracks are electrons.

Initial simulations were for electron beams incident on a tungsten cylinder with 150 mm radius and 351 mm thickness to determine the shower profile. The thickness is a multiple of the radiation length of tungsten, which is 3.504 mm. The depths of 35.1 cm of fundamental tungsten will not actually occur in a collider, due to practical engineering considerations (cooling, mounts, purity, etc.) and cost (which is a result of planetary abundance considerations). It is also unlikely that collimating masks would be 35 cm thick, though in the interaction region shielding cone, it is possible to encounter depths of that order.

In order to map out the shower profiles, the simulations included 43 virtual detectors, 39 of which were internal to the tungsten cylinder. The internal virtual

detectors were placed at multiples of the tungsten radiation length (3.5 mm). The remaining four virtual detectors were placed around the cylinder to ensure hermeticity of detection. One of the external virtual detectors is “beam detector” which sits in the incident particle beam and plugs the “bore hole” left in the backscatter detector. A schematic is shown in Figure 15.

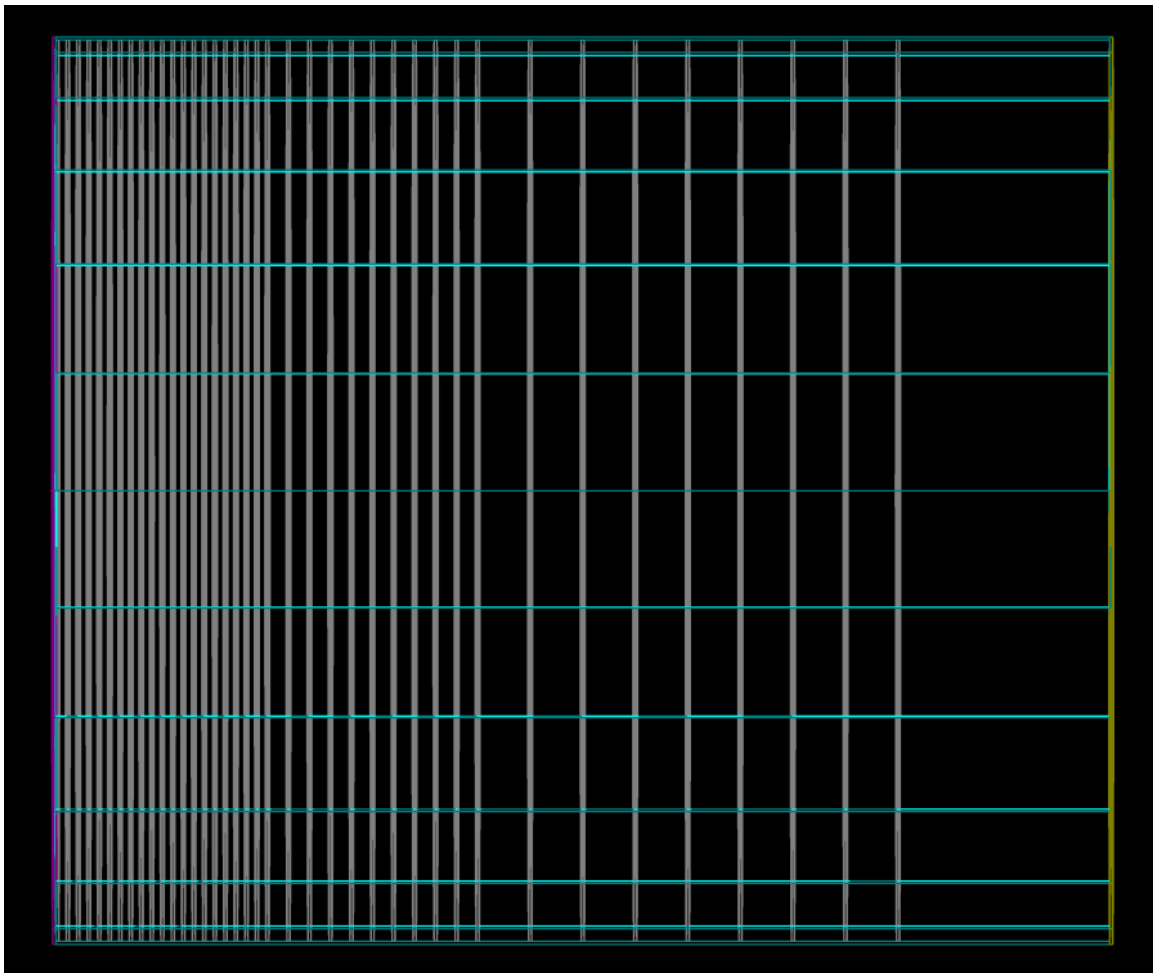

Figure 15: Simple geometry used in electromagnetic shower profiling.
The gray planes are virtual detectors, the teal represents the target cylinder, the magenta is a backscatter detector, and the gold is the punch-through detector. The sidescatter detector is not visible in this image.

The vast majority of secondary particles from electron-on-target collisions can be grouped into four classes: gamma rays, [tertiary] electrons, positrons, and neutrons. Electron and positron fluence peaks near ten radiation lengths while the gamma fluence (defined here as counts per detector) peaks near eleven radiation lengths as expected due to the additional bremsstrahlung contribution from tertiary electrons and positrons. As shown in Figure 16, the neutron fluence peak occurs around twelve radiation lengths (4.2 cm) for 25 GeV incident electrons and increases to 17 radiation lengths (6.0 cm) for 750 GeV incident electrons.

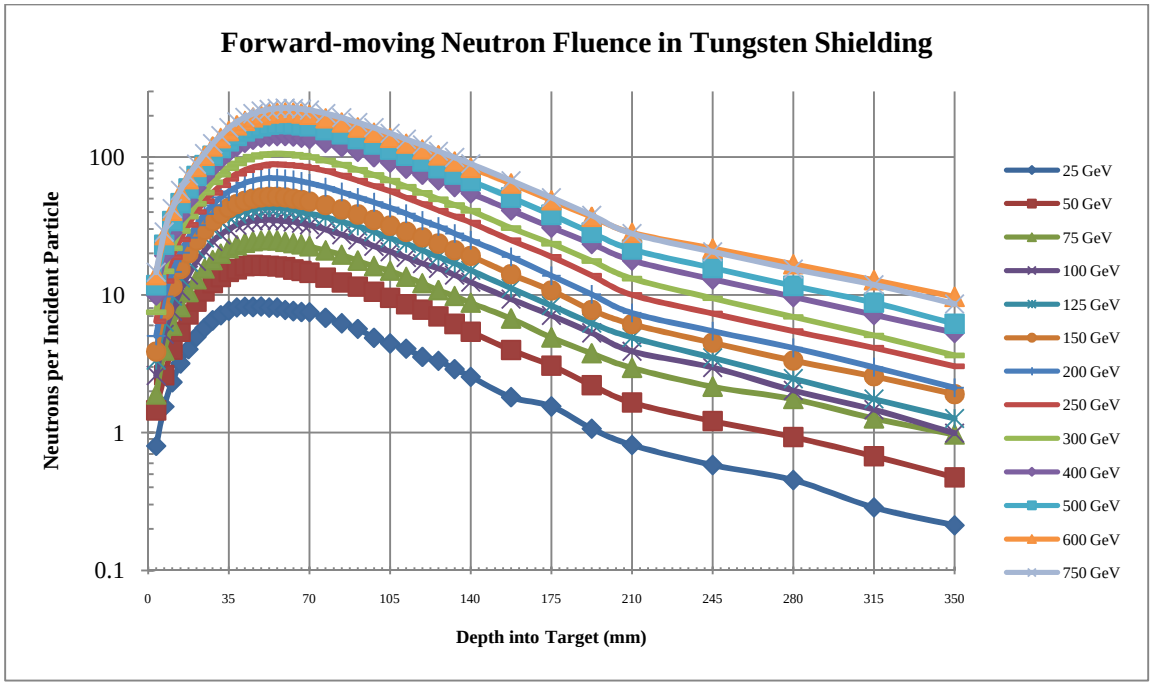

Figure 16: Normalized forward-moving neutron fluences for various electron beam energies.
The electron energies follow a boosted Michel distribution.

The nuclear interaction length (also known as nuclear absorption length) of tungsten in 9.946 cm and the nuclear collision length is 5.719 cm. It can be expected that

the peak for forward-moving neutron fluences will not appreciably increase beyond the nuclear collision length, even at higher energies.

3.4 Neutron Absorption

The standard methods to absorb free neutrons are to use borated polyethylene (BPE or polyboron), polylithium, or cadmium. With regards to boron (and lithium), the polyethylene ($(C_2H_2)_n$) slows high-energy neutrons into the thermal region (thermalizes) so that the boron (lithium) can then capture them. Boron has two stable isotopes, ^{10}B and ^{11}B, whose abundances are 19.9% and 80.1%, respectively, but only ^{10}B is an efficient neutron absorber though the $n^0 + {}^{10}B \rightarrow {}^{4}He + {}^{7}Li\ (+\gamma)$ reaction.

To test neutron absorption, a series of simulations were done. The first set of simulations were electron beams incident on a 36-mm thick tungsten disc used as a spallation source with a 1.8-meter long cylinder of borated polyethylene (either 5% or 30% boron) immediately behind it. These percentages were chosen based on their commercial availability. To ensure maximum accuracy, we employed the QGSP_BERT_HP physics engine. This setup is shown in Figure 17.

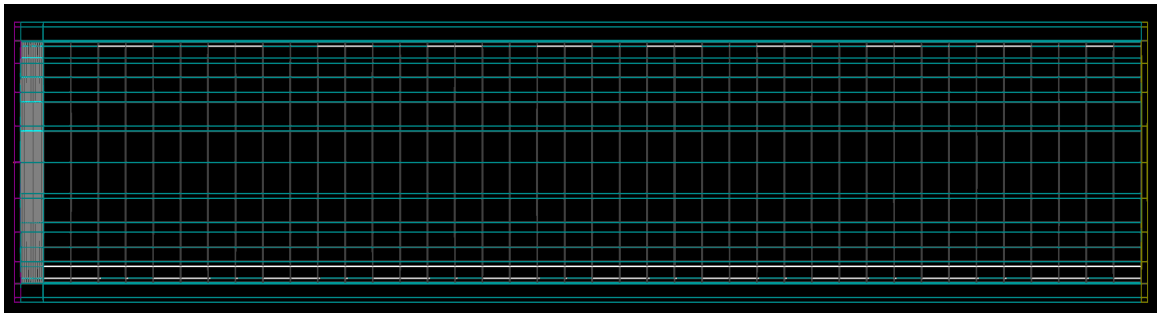

Figure 17: BPE simulation setup.
A tungsten spallation target and a 1.8-meter thick BPE absorber with regularly-placed virtual detectors.

The BPE was created in G4beamline as a mixture of polyethylene and naturally-occurring boron rather than ^{10}B-enriched boron. This material creation was required as G4beamline employs the G4Material class which in turn uses a NIST materials database for predetermined materials, of which borate polyethylene is not included. MARS, on the other hand, does include borated polyethylene as a pre-programmed material.

The main result of these simulations was to show that the lower boron concentration was slightly more efficient at absorbing neutrons, likely as a result of the higher polyethylene content. This is shown in Figure 18, below, for 200 GeV electrons incident on the target as shown in Figure 17. The polyethylene, of course, is responsible for the thermalization of neutrons due to its low-Z material content. Additionally, the carbon in polyethylene will also absorb neutrons, though with a lower cross section than boron. However, at first glance, this result was counter-intuitive so we began an examination of the nuclear properties within GEANT4.

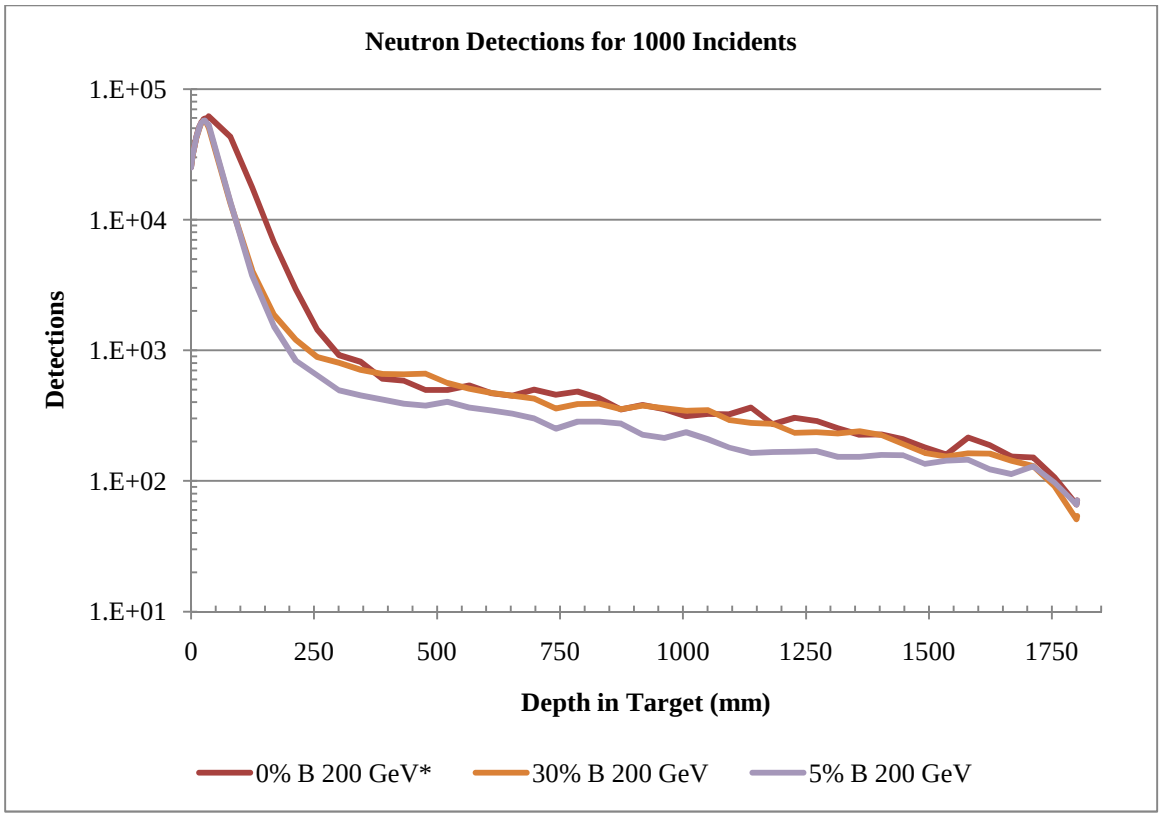

Figure 18: Neutron detections for 1000 incident 200-GeV electrons.
This figure shows the neutron detections through Figure 17 for varying proportions of boron in polyethylene.

In the process of examining that, we looked at the boron isotopic cross sections within the GEANT4 data files themselves. GEANT4 isotopic data nominally comes from the National Nuclear Data Center (NNDC) at Brookhaven National Laboratory, but a comparison of the GEANT4 data files with NNDC plots showed a number of differences.

The G4NDL3.14 data files are divided into a number of subdirectories, only three of which are applicable to boron: Capture, Inelastic, Elastic. Within each of these subdirectories are Crosssection directories which contain data files like 5_10_Boron or 5_11_Boron (Z_A_Name format) which are formatted such that cross sections (σ) and energies are given in barns and eV, respectively.

For elastic scattering cross sections at low energies ($< 0.1\ eV$), GEANT4 assumes a flat cross section for both ^{10}B and ^{11}B; whereas the cross sections exponentially increase at lower energies for both. For inelastic scattering, GEANT4 shows ^{11}B to have a higher cross section than ^{10}B above 10 MeV, as seen in Figure 19. This directly contradicts NNDC data which shows the cross section of ^{10}B to be always above that of ^{11}B and that the difference between cross sections should be increasing above 10 MeV, as seen in Figure 20.

However, it was found that GEANT4 is missing the so-called "quasi-elastic" scattering cross section (which applies to $n^0 + {}^{11}B \rightarrow n^0 + {}^{4}He + {}^{7}Li$), which accounts for a 40% discrepancy in the cross section for ^{11}B. The quasi-elastic interaction with ^{11}B causes the neutron to slow and change direction, thus increasing the chance that it is absorbed or further thermalized.

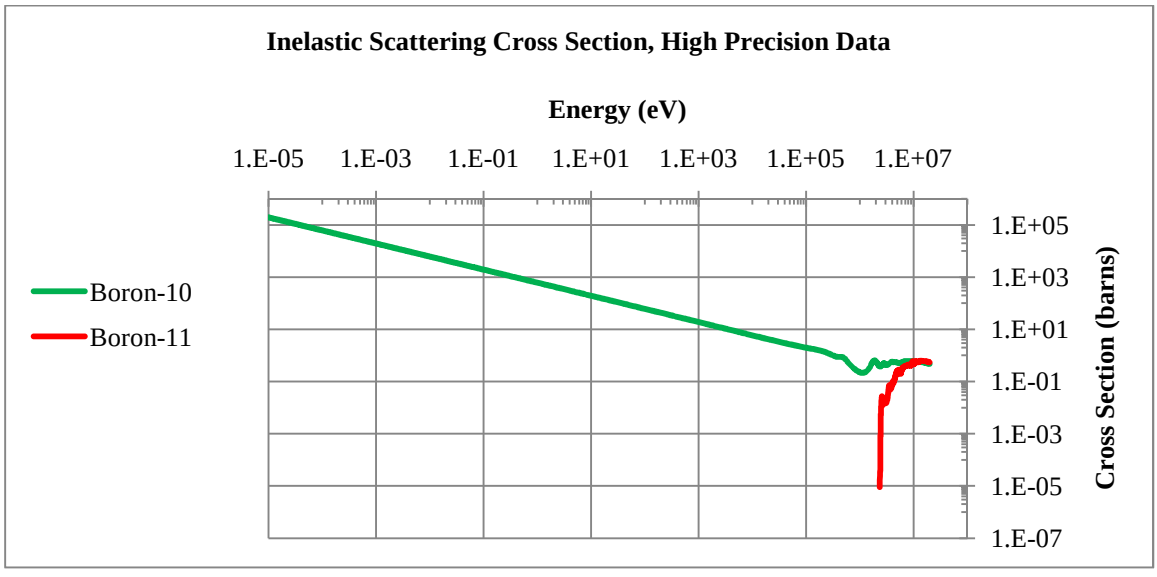

Figure 19: Inelastic neutron scattering cross sections for ^{10}B and ^{11}B from G4NDL (version 3.14).

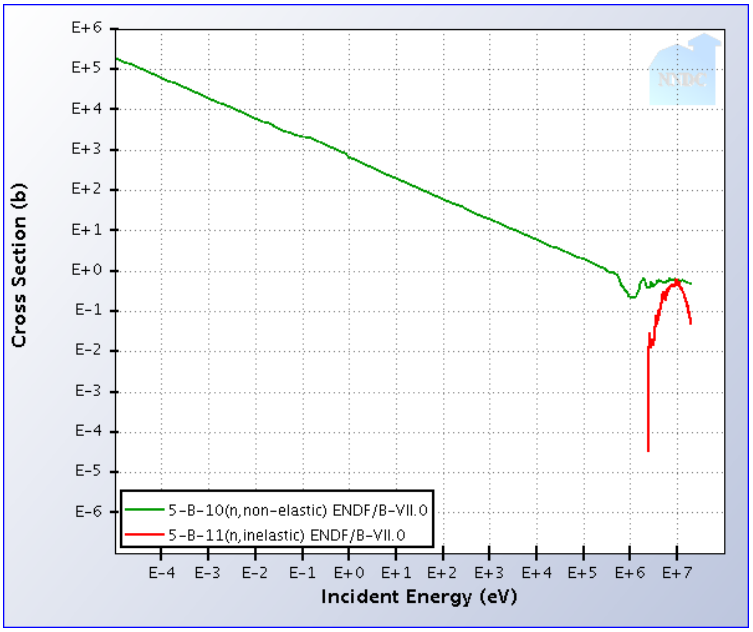

Figure 20: Inelastic neutron scattering cross sections for ^{10}B and ^{11}B.

There also appears to be a systematic issue in GEANT4 where ^{10}B neutron capture, $^{10}B + {}^{1}n \rightarrow {}^{7}Li + {}^{4}He$, is not properly implemented. It was determined by D. Hedin that GEANT4 implements neutron capture as $^{10}B + {}^{1}n \rightarrow {}^{8}Li + {}^{3}He$ and $^{10}B + {}^{1}n \rightarrow {}^{7}Li + {}^{4}He + \gamma$. However, the substitution of ^{8}Li for ^{7}Li and ^{3}He for ^{4}He, while incorrect in terms of the nuclear reaction, probably does not matter to the simulation as the daughter nuclei will range out before interacting with an accelerator or detector component. Additionally, the gamma that results approximately 95% of the time is less than half of an MeV (0.48 MeV), and can be effectively ignored.

Boron enrichment is also problematic, as a user cannot specify a single isotope of boron via the G4beamline "materials" command, but rather must alter the data files within the G4NDL3.14 directories. This is currently under investigation by T. Roberts.

3.5 Muon Background

One of the main backgrounds for a muon collider is from non-beam (but beam-associated) muons that enter the detector volume. These muons can be produced though Bethe-Heitler pair production, electron-positron annihilation, or photopion production (pion decay). (Keller 1991)

Particle pair production can occur in three types of interactions: virtual photon propagation, di-photon, or photon-nucleus (photonuclear) creation. Virtual photon propagation, such as , requires the annihilation of a particle and its antiparticle to a virtual photon which then pair produces as shown in Figure 21.

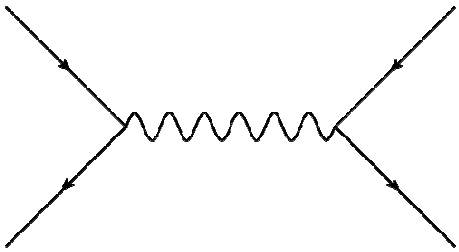

Figure 21: Tree-level Feynman diagram of s-channel pair annihilation-pair production.

The diphoton pair production process (Figure 22), exemplified by photon-photon to lepton-antilepton ( ) is required for conservation of 4-momentum in free space. This can be considered as a negligible contribution within the beamline of a muon collider when compared to the other processes.

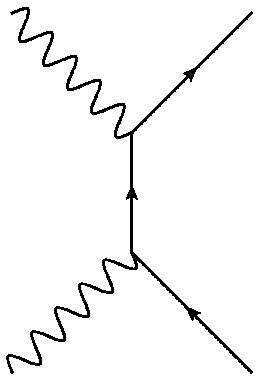

Figure 22: Example di-photon pair production Feynman Diagram at tree level.

The last process, wherein the external photon interacts with the virtual photons within the Coulomb field of the nucleus to pair produce some particle , is known as Bethe-Heitler production, after Hans A. Bethe and Walter H. Heitler. This process is shown in Figure 23. (Bethe & Heitler 1934)

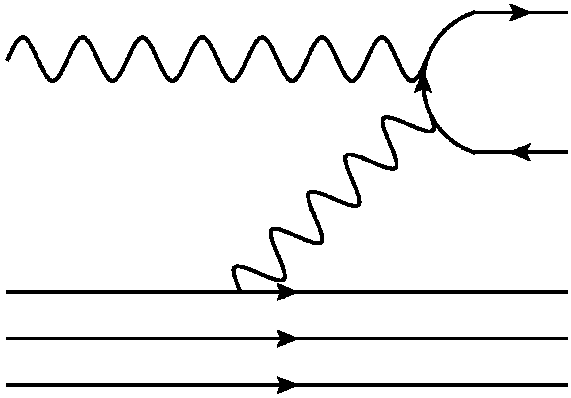

Figure 23: Example Bethe-Heithe pair production.

The production cross section (in barns) can be stated as

$$\sigma = \frac{28}{9} Z^2 \alpha r_f^2 \left(ln\left(\frac{2\hbar\omega}{m_f c^2}\right) - \frac{109}{42}\right)$$

where Z is the atomic number, α is the fine structure constant, r_f is the classical fermion radius, m_f is the mass of the fermion, and $\hbar\omega$ is the energy of the incident photon. The classical fermion radius is given by

$$r_f = \frac{e^2}{m_f c^2}$$

where e is the elementary charge and $m_f c^2$ is the rest-mass energy of the fermion.

For muon pair production, we use $r_\mu = r_e \frac{m_e}{m_\mu}$ wherein m_e and m_μ are the rest masses of the electron and muon, respectively. This makes the production cross section

$$\sigma = \frac{28}{9} Z^2 \alpha \left(r_e^2 \frac{m_e^2}{m_\mu^2}\right)\left(\ln\left(\frac{2E_\gamma}{m_\mu}\right) - \frac{109}{42}\right).$$

Here again we see the ratio of electron and muon masses, squared, which is $\sim 1/42{,}000$. Obviously muon pair production will be less than electron pair production (which is, of course, another source of electrons and positrons), but these muons could affect physics studies as they could pass through shielding material and enter the detector volume.

As a consistency check, we followed the example of Ziemann and used this calculation for photons incident on a thin iron target and compared this to the GEANT4 content. (Ziemann 2008)

Initial simulations demonstrated that muon pair production is not activated by default in G4beamline. There is a physics process "MuPairProd" that is active, but this is not actually Bethe-Heitler production. The most recent version of G4beamline, version

2.08, has an additional physics process that can be activated, specifically "gammaToMuPair," in order to force Bethe-Heitler muon production to occur. The argument for this process can also be used to specify a scale factor in order to increase the Bethe-Heitler cross section so as to reduce the number of required incident events. This is a useful addition as Bethe-Heitler production is a rare process, as shown in Appendix D.

With this process activated, G4beamline produces muon pairs for photon energies above 1 GeV. Simulations at 1 GeV did not show any Bethe-Heitler production. Simulations at 10 GeV did, however. It should be noted that the cross section calculation assumes the ultra-relativistic limit wherein $E_\gamma >> m_\mu$.

G4beamline shows a consistent deficit in Bethe-Heitler muon pairs produced when compared to Bethe and Heitler's original calculations. This is shown in Figure 24 and Figure 25 for iron and tungsten, respectively. One correction is that the original 1930s cross section calculation overestimates the production cross section for high-Z materials by approximately 10%. (Bethe & Maximon 1954) However, even this correction does not fit the G4beamline simulation data, as evidenced in Figure 25.

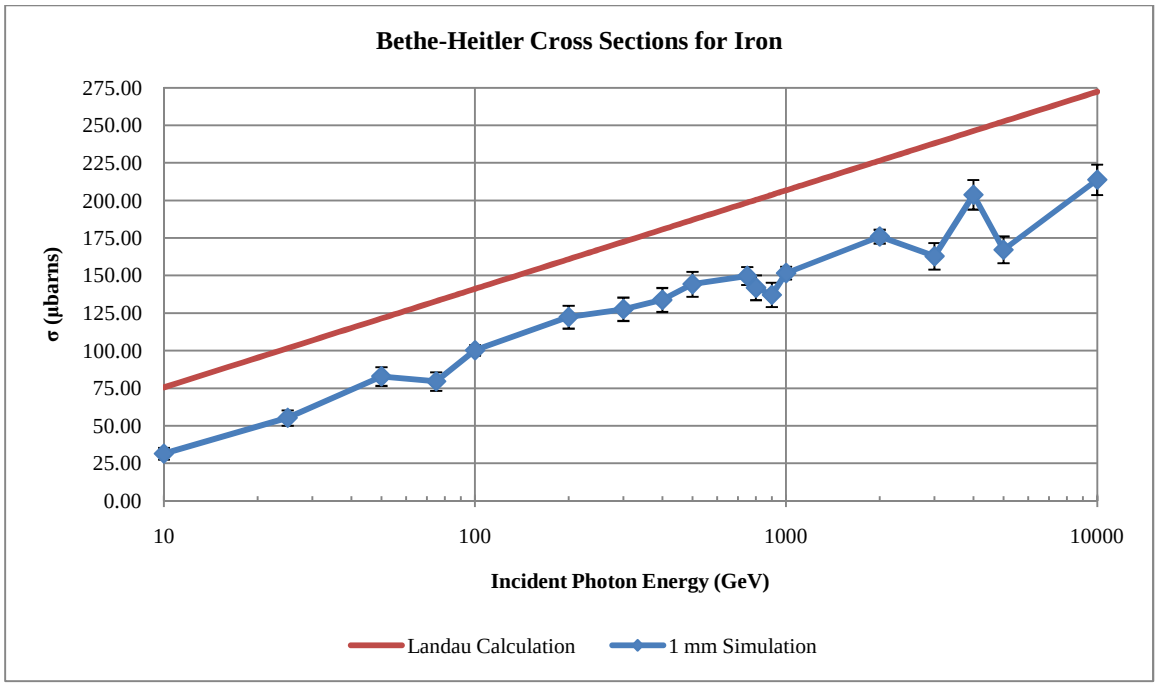

Figure 24: Bethe-Heitler cross sections for iron based on G4beamline simulations and Landau and Lifshitz calculation.

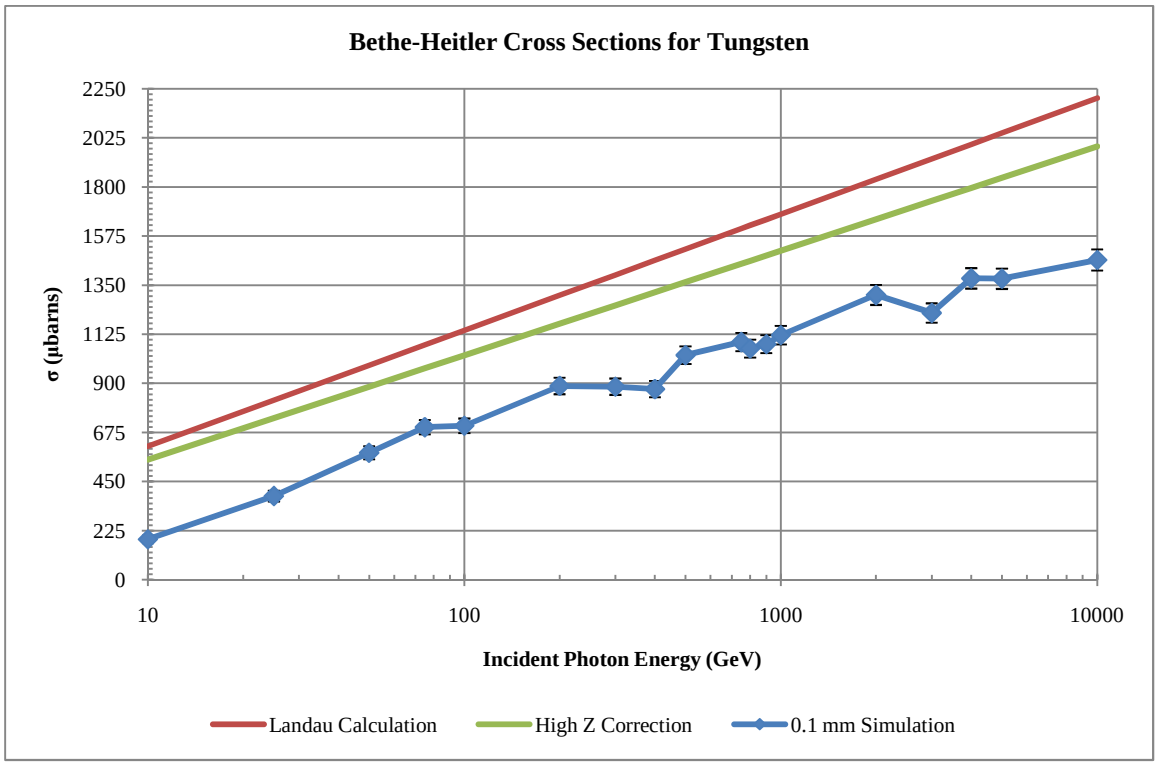

Figure 25: Bethe-Heitler cross sections for iron based on G4beamline simulations and Landau and Lifshitz calculations.

The deficit compared to the original calculation was confirmed for iron at 100 GeV incident photons at two thickness (0.5 and 2.0 mm) in addition to the standard 1.0 mm runs.

An literature search revealed that GEANT4 parameterizes Bethe-Heitler muon production with the following equation

$$\sigma_{par} = \frac{28}{9}\alpha\, Z^2 r_c^2 \ln\left(1 + W_M C_f E_g\right)$$

where again α is the fine structure constant, Z is the atomic number, and r_c is the classical [muon] radius. The terms in the logarithm are additional factors that correct the cross section as functions of energy.

W_M is the slope of the cross section (as a function of energy) for energies greatly above the threshold energy.

$$W_M = \frac{1}{4\, D_n \sqrt{e} m_\mu}$$

where $\sqrt{e}$ is the square root of Euler's number $\left(\sqrt{e} \approx 1.64872127 \ldots\right)$, m_μ is the muon rest mass, and D_n is a correction factor related to the nuclear composition of a material.

$$D_n = \begin{cases} 1.49 & for\ Hydrogen \\ 1.54\, A^{0.27} & for\ all\ else \end{cases}$$

where A is the atomic mass number.

C_f is an empirical correction factor for lower energies which is

$$C_f = \left[1 + 0.04 \ln\left(1 + \frac{E_c}{E_\gamma}\right)\right]$$

where E_γ is the photon energy (in GeV) and E_C is the critical energy, given by

$$E_C = \left[-18 + \frac{4347}{BZ^{-\frac{1}{3}}}\right] GeV$$

where Z is the atomic number and B is another element-specific parameter given by

$$B = \begin{cases} 202.4 & for\ Hydrogen \\ 183 & for\ all\ else \end{cases}.$$

E_g is the threshold behavior given by

$$E_g = \left(1 - \frac{4m_\mu}{E_\gamma}\right)^t \left(W_{sat}^s + E_\gamma^s\right)^{\frac{1}{s}}$$

where again m_μ and E_γ are the muon rest mass and the incident photon energy. W_{sat} is a coefficient related to bremsstrahlung saturation and is given by

$$W_{sat} = B\ Z^{-\frac{1}{3}} \frac{4\sqrt{e}m_\mu^2}{m_e}$$

where m_e is the electron rest mass.

The quantities s and t are parameters given by

$$t = 1.479 + 0.00799 D_n$$

$$s = -0.88$$

Plugging this all in gets

$$\sigma_{par} = \frac{28}{9}\alpha\, Z^2 \left(r_e^2 \frac{m_e^2}{m_\mu^2}\right) \ln\left\{1 + \left(\frac{1}{6.16\, A^{0.27}\, \sqrt{e}\, m_\mu}\right)\right.$$

$$\cdot \left(1 + 0.04 \ln\left(1 + \frac{-18 + \frac{4347}{183\, Z^{-\frac{1}{3}}}}{E_\gamma}\right)\right)$$

$$\cdot \left(\left(1 - \frac{4m_\mu}{E_\gamma}\right)^{1.479 + 0.0123046\, A^{0.27}} \left(\left(B\, Z^{-\frac{1}{3}} \frac{4\sqrt{e}\, m_\mu^2}{m_e}\right)^{-0.88}\right.\right.$$

$$\left.\left.\left. + E_\gamma^{-0.88}\right)^{-\frac{1}{0.88}}\right)\right\}$$

where all relevant quantities are calculated in GeV.

This parameterization equation does fit the Monte Carlo data (as it should, since GEANT4 uses that parametrization to calculate Bethe-Heitler cross sections), within the range of error bars, as shown in Figure 26 and Figure 27.

The differences between Bethe and Heitler's original work in the 1930s and the GEANT4 parametrization are mainly accounted for by higher-order corrections. Among these corrections are a better understanding of muon bremsstrahlung at higher muon energies, application of the finite size of a nucleus, and corrections for electromagnetic screening of the nucleus by electrons. (Burkhardt *et al*. 2002) Additionally, the GEANT4 parameterization includes some empirical correction factors to account for experimental results.

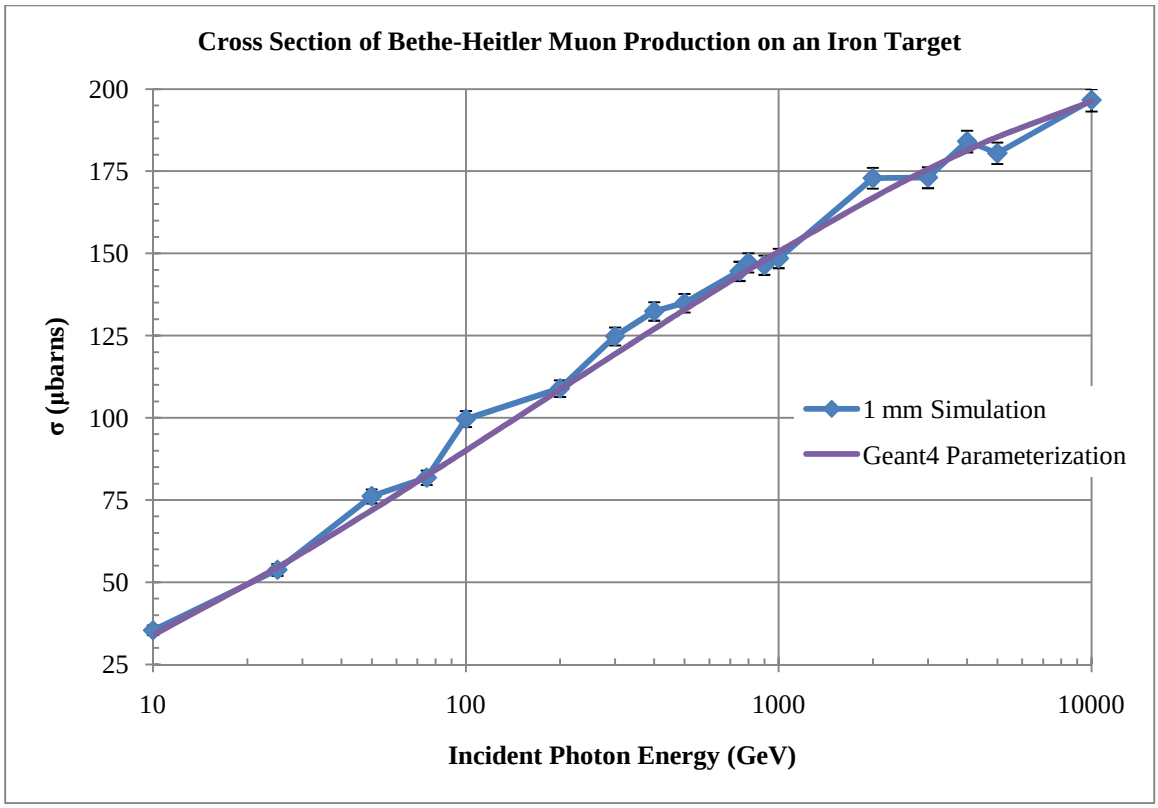

Figure 26: Cross sections for Bethe-Heitler muon production on an iron target.

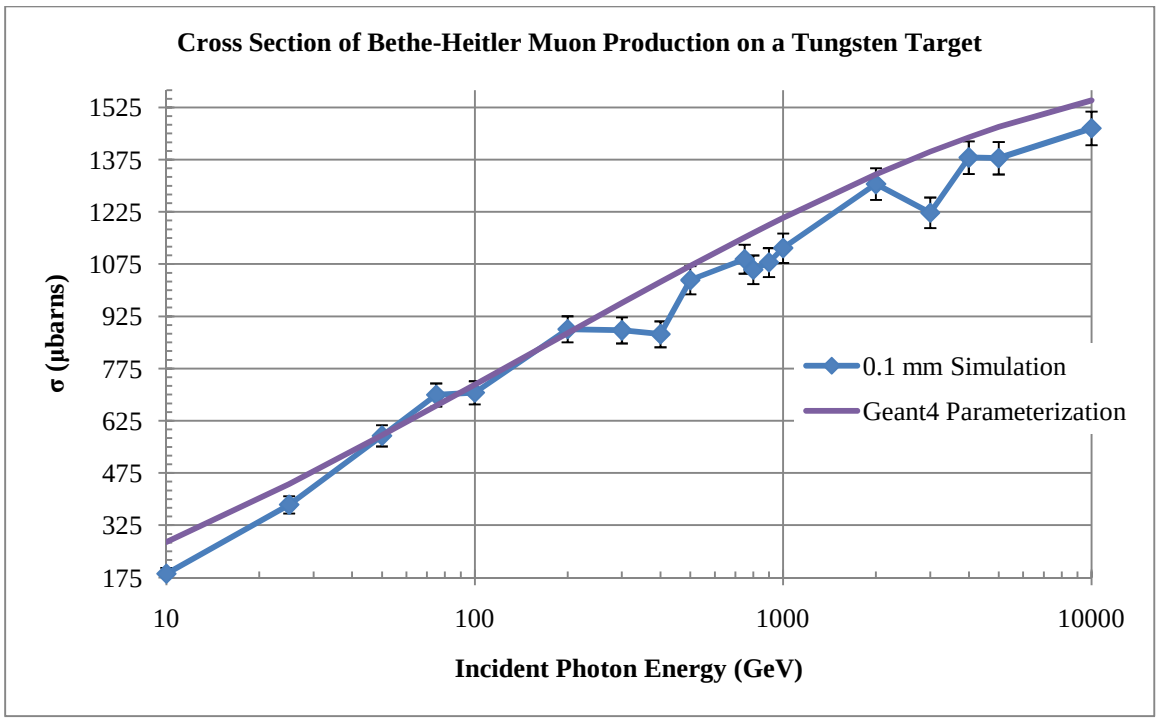

Figure 27: Cross sections for Bethe-Heitler muon production on an iron target.

Photopion production $\left(\gamma\, A \rightarrow X\, \pi\, \left(\pi \rightarrow \mu\, \nu_{\mu}\right)\right)$ has a similar cross section to Bethe-Heitler production, but these pions will likely interact before decaying. (Keller 1991) This background is beyond the scope of this project. However, it must be noted that in GEANT4 there is a known problem wherein the branching ratio of the rare pion decay ($\pi^{\pm} \rightarrow e^{\pm}\nu_e$) is assumed to be zero. This, of course, would artificially increase the muon production rate in front-end simulations by a small amount. G4beamline corrects for rare pion decay. (Roberts 2011)

CHAPTER 5:

CONCLUSION

"I just finished thinking about something, and didn't start thinking about anything else."

Private Michael J. Caboose, Red vs. Blue

Initial validation studies of a few muon collider physics background processes using G4beamline have been undertaken and results presented. While these investigations have revealed a number of hurdles to getting G4beamline up to the level of more established simulation suites, such as MARS, the close communication between us, as users, and the G4beamline developer, Tom Roberts, has allowed for rapid implementation of user-desired features. The main example of user-desired feature implementation, as it applies to this project, is Bethe-Heitler muon production.

Regarding the neutron interaction issues, we continue to study the specifics of how GEANT4 implements nuclear interactions. The GEANT4 collaboration has been contacted regarding the minor discrepancies in the neutron interaction cross sections for boron. While corrections to the data files themselves are simple to implement and distribute, it is quite possible, however, that coding changes may be required in G4beamline or even in GEANT4 to fully correct nuclear interactions. Regardless, these studies are ongoing and future results will be reflected in updated releases of G4beamline.

BIBLIOGRAPHY

Ankenbrandt, C. M., Atac, M., Autin, B., Balbekov, V. I., Barger, V. D., Benary, O., Berg, J. S., Berger, M. S., Black, E. L., Bogacz, A. B. S. A., Bolton, T., Caspi, S., Celata, C., Chou, W., Cline, D. B., Corlett, J., Cremaldi, L., Diehl, H. T., Drozhdin, A., Fernow, R. C., Finley, D. A., Fukui, Y., Furman, M. A., Gabriel, T., Gallardo, J. C., Garren, A. A., Geer, S. H., Ginzburg, I. F., Green, M. A., Guler, H., Gunion, J. F., Gupta, R., Han, T., Hanson, G. G., Hassanein, A., Holtkamp, N., Johnson, C., Johnstone, C., Kahn, S. A., Kaplan, D. M., Kim, E. S., King, B. J., Kirk, H. G., Kuno, Y., Lebrun, P., Lee, K., Lee, P., Li, D., Lissauer, D., Littenberg, L. S., Lu, C., Luccio, A., Lykken, J. D., McDonald, K. T., McInturff, A. D., Miller, J. R., Mills, F. E., Mokhov, N. V., Moretti, A., Mori, Y., Neuffer, D. V., Ng, K.-Y., Noble, R. J., Norem, J. H., Onel, Y., Palmer, R. B., Parsa, Z., Pischalnikov, Y., Popovic, M., Prebys, E. J., Qian, Z., Raja, R., Reed, C. B., Rehak, P., Roser, T., Rossmanith, R., Scanlan, R. M., Sessler, A. M., Schadwick, B., Shu, Q.-S., Silvestrov, G. I., Skrinsky, A. N., Smith, D., Spentzouris, P., Stefanski, R. J., Striganov, S., Stumer, I., Summers, D. J., Tcherniatine, V., Teng, L. C., Tollestrup, A. V., Torun, Y., Trbojevic, D., Turner, W. C., Vahsen, S. E., Van Ginneken, A., Vsevolozhskaya, T. A., Wan, W., Wang, H., Weggel, R., Willen, E. H., Wilson, E. J. N., Winn, D. R., Wurtele, J. S., Yokoi, T., Zhao, Y., Zolotorev, M. 1999. "Status of muon collider research and development and future plans." *Physics Review Special Topics – Accelerators and Beams* 2:081001.

Ankenbrandt, C., Alexahin, Y., Balbekov, V., Barzi, E., Bhat, C., Brommelsiek, D., Bross, A., Burov, A., Drozhdin, A., Finley, D., Geer, S., Gelfand, N., Gianfelice-Wendt, E., Hu, M., Jansson, A., Johnstone, C., Johnstone, J., Kashikhin, Vl., Kashikhin, V., Lamm, M., Lebedev, V., Mokhov, N., Moore, C., Moretti, A., Neuffer, D., Ng, K.-Y., Popovic, M., Rakhno, I., Shiltsev, V., Spentsouris, P., Striganov, A., Tollestrup, A., Valishev, A., Van Ginneken, A., Yonehara, K., Yoshikawa, C., Zlobin, A., Norem, J., Berg, J. S., Gallardo, J. C., Gupta, R., Kirk, H., Palmer, R., Fernow, R., Wanderer, P., Bogacz, A., Chao, Y.-C., Derbenev, Y., Rimmer, R. A., Sabbi, G., Ferracin, P., Caspi, S., Zisman, M., Abrams, R., Beard, K., Johnson, R. P., Cummings, M. A., Kahn, S. A., Korenev, S., Newsham, D., Roberts, T. J., Cline, D. B., Fukui, Y., Garren, A., Hanson, G., Klier, A., Cremaldi, L. M., Summers, D. J. 2008. "Muon Collider Task Force Report." *Fermilab-TM-2399-APC*.

Ankenbrandt, C., Bogacz, S. A., Bross, A., Geer, S., Johnstone, C., Neuffer, D., Popovic, M. 2009. "Low-energy neutrino factory design." *Physical Review Special Topics – Accelerators and Beams* 12:070101.

Baur, G., Leuschner, A. 1999. "Bethe-Heitler cross-section for very high photon energies and large muon scattering angles." *The European Physical Journal C* 8:631-635.

Benary, O., Kahn, S., Stumer, I. 2000. "Detector Backgrounds for a High Energy Muon Collider." *AIP Conference Proceedings* 530:1-12.

Berestetskii, V. B., Lifshitz, E. M., Pitaevskii, L. P. (Trans. Sykes, J. B., Bell, J. S.) 1982. *Quantum Electrodynamics, 2nd Edition*. Pergamon Press, Oxford.

Bethe, H. A., Heitler, W. 1934. "On the Stopping of Fast Particles and on the Creation of Positive Electrons." *Proceedings of the Royal Society of London, Series A* 146:83-112.

Bethe, H. A., Maximon, L. C. 1954. "Theory of Bremsstahlung and Pair Production. I. Differential Cross Section." *Physical Review* 93:768-784.

Bether, H. A. 1996. *Selected Works of Hans A. Bethe With Commentary*. World Scientific, Singapore.

Bradt, Hale. 2004. *Astronomy Methods: A Physical Approach to Astronomical Observations*. Cambridge University Press, Cambridge.

Burkhardt, H., Kelner, S. R., Kokoulin, R. P. 2002. "Monte Carlo Generation for Muon Pair Production." *CERN-SL-2002-016 (AP)*. Geneva, Switzerland.

Christenson, J. H., Hicks, G. S., Lederman, L. M., Limon, P. J., Pope, B. G., Zavattini, E. 1973. "Observation of Muon Pairs in High-Energy Hadron Collisions." *Physical Review D* 8:2016-2034.

Cline, D. B. 1996. "Some Comments on the Early History of the $\mu^+\mu^-$ Concept and the High Intensity μ Storage Ring." *AIP Conference Proceedings* 352:3-6.

Edwards, D. A., Syphers, M. J. 2004. *An Introduction to the Phyiscs of High Energy Accelerators*. WILEY-VCH Verlag GmbH & Co., Weinheim, Germany.

Fasso, A., Ferrari, A., Ranft, , J., Sala, P. R. 2011. "FLUKA-2011 Manual." Retrieved from http://www.fluka.org/content/manuals/fluka2011.manual.

G4beamline. 2011. Retrieved from http://g4beamline.muonsinc.com.

GEANT4. 2011. Retrieved from http://geant4.cern.ch. (Specifically, http://geant4.web.cern.ch/geant4/support/about.shtml, http://geant4.cern.ch/support/download.shtml, http://geant4.cern.ch/support/proc_mod_catalog/physics_lists/referencePL.shtml.)

GEANT4 collaboration (Agostinelli, S., Allison, J., Amako, K., Apostolakis, J., Araujo, H., Arce, P., Asai, M., Axen, D., Banerjee, S., Barrand, G., Behner, F., Bellagamba, L., Boudreau, J., Broglia, L., Brunengo, A., Burkhardt, H., Chauvie, S., Chuma, J., Chytracek, R., Cooperman, G., Cosmo, G., Degtyarenko, P., Dell'Acqua, A., Depaola, G., Dietrich, D., Enami, R., Feliciello, A., Ferguson, C., Fesefeldt, H., Folger, G., Foppiano, F., Forti, A., Garelli, S., Giani, S., Giannitrapani, R., Gibin, D., Cadenas, J. J. G., Gonzalez, I., GraciaAbril, G., Greeniaus, L. G., Greiner, W., Grichine, V., Grossheim, A., Gumplinger, P., Hamatsu, R., Hashimoto, K., Hasui, H., Heikkinen, A., Howard, A., Ivanchenko, V., Johnson, A., Jones, F. W., Kallenbach, J., Kanaya, N., Kawabata, M., Kawabata, Y., Kawaguti, M., Kelner, S., Kent, P., Kodama, T., Kokoulin, R., Kossov, M., Kurashige, H., Lamanna, E., Lampen, T., Lara, V., Lefebure, V., Lei, F., Liendl, M., Lockman, W., Longo, F., Magni, S., Maire, M., Medernach, E., Minamimoto, K., MoradeFreitas, P., Morita, Y., Murakami, K., Nagamatu, M., Nartallo, R., Nieminen, P., Nishimura, T., Ohtsubo, K., Okamura, M., O'Neale, S., Oohata, Y., Paech, K., Perl, J., Pfeiffer, A., Pia, M. G., Ranjard, F., Rybin, A., Sadilov, S., DiSalvo, E., Santin, G., Sasaki, T., Savvas, N., Sawada, Y., Scherer, S., Sei, S., Sirotenko, V., Smith, D., Starkov, N., Stoecker, H., Sulkimo, J., Takahata, M., Tanaka, S., Tcherniaev, E., SafaiTehrani, E., Tropeano, M., Truscott, P., Uno, H., Urban, L., Urban, P., Verderi, M., Walkden, A., Wander, W., Weber, H., Wellisch, J. P., Wenaus, T., Williams, D. C., Wright, D., Yamada, T., Yoshida, H., Zschiesche, D.) 2003. "GEANT4 – a simulation tooklit." *Nuclear Instruments and Methods in Physics Research Section A: Accelerators, Spectrometers, Detectors and Associated Equipment* 506: 250-303.

Geer, S. 2009. "Muon colliders and Neutrino Factories." *Annual Reviews of Nuclear and Particle Science* 59:347-365.

Gianfelice-Wendt, E. 2010. Private communication.

Jackson, J. D. 1999. *Classical Electrodynamics: Third Edition*. John Wiley & Sons, Inc., Hoboken, NJ.

Kahn, S. A., Cummings, M. A. C., Hedin, D., Morris, A. O., Kozminski J. F. 2011. "Beam Induced Detector Backgrounds at a Muon Collider." *Proceedings of the 2011 Particle Accelerator Conference*. New York, NY.

Keller, L. P. 1991. "Calculations of Muon Background in a 0.5 TeV Linear Collider." *SLAC-PUB-5533*.

Kelner, S. R., Kokoulin, R. P., Petrukhin, A. A. 1995. "About Cross Section for High-Energy Muon Bremsstrahlung." *Moscow State Engineering Physics Institute Preprint* 024-95.

Kim, K. J., Tsai, Y.-S. 1973. "Improved Weizsäcker-Williams Method and Its application to Lepton and W-Boson Pair Production." *Physical Review D* 8:3109-3125.

MAP Collaboration. 2010. Retrieved from http://map.fnal.gov/muon-collider/graphics.shtml.

Martin, S. 2011. *Phenomenology of Particle Physics: NIU Spring 2011 PHYS 686 Lecture Notes*. DeKalb, IL.

Mokhov, N. V., James, C. C. 2011. "The MARS Code System User's Guide Version 15 (2010)." Batavia, IL.

Morris, A. O., Hedin, D., Cummings, M. A. C., Kahn, S. A., Roberts T. J., Kozminski J. F. 2011. "Physics Validation of Monte Carlo Simulations for Detector Backgrounds at a Muon Collider." *Proceedings of the 2011 Particle Accelerator Conference*. New York, NY.

Nakamura, K. *et al*. (Particle Data Group). 2010. *Journal of Physics G* 37:075021.

National Nuclear Data Center. 2011. Retrieved from http://www.nndc.bnl.gov.

Neuffer, D. 1979. "Colliding Muon Beams at 90 GeV." *FN-319 2252.000*. Batavia, IL.

Neuffer, D. 1986. "Multi-TeV Muon Colliders." *AIP Conference Proceedings* 156:201-208.

Neuffer, D. V. 1994. "$\mu^+ - \mu^-$ colliders: possibilities and challenges." *Nuclear Instruments and Methods in Physics Research A* 350:27-35.

Neuffer, D. 1999. "$\mu^+ - \mu^-$ Colliders." *CERN 99-12*. Geneva, Switzerland.

Noble, R. J. 1993. "Particle Production and Survival in Muon Acceleration." *AIP Conference Proceedings* 279:949-957.

Palmer, R., Tollestrup, A., Sessler, A., Skrinsky, A., Ankenbrandt, C., Baltz, A., Barger , V., Benary , O., Berger , M., Bogacz , A., Caspi, S., Chen, P., Cheng, W.-H., Cho, Y., Cline, D., Courant, E., Ehst, D., Fernow, R., Furman, M., Gallardo, J., Garren, A., Geer, S., Ginzburg, I., Gordon, H., Green, M., Griffin, J., Gunion, J., Gupta, R., Hershcovitch, A., Han, T., Johnstone, C., Kahn, S., Kahana, D., Kirk, H., Kycia, T., Lebrun, P., Lee, Y., Lissauer, D., Littenberg, L., Luccio, A., Ma, H., McInturff, A., Mills, F., Mokhov, N., Moretti, A., Morgan, G., Muhlbauer, M., Murtagh, M., Neuffer, D., Ng, K-Y., Noble, R., Norem, J., Norum, B., Novitski, I., Oide, K., Paige, F., Parsa, Z., Peterson, J., Polychronakos, V., Popovic, M., Protopopescu, S., Qian, Z., Rehak, P., Roser, T., Rossmanith, R., Scanlan, R., Schachinger, L., Shu, Q.-S., Silvestrov, G., Simrock, S., Stumer, I., Summers, D., Syphers, M., Takahashi, H., Takai, H., Tchernatine, V., Torun, Y., Trbojevic, D., Turner, W., Van Ginneken, A., Vsevolozhskaya, T., Weggel, R., Willen, E., Willis, W., Winn, D., Wurtele, J., Zhao, Y. 1996. "$\mu^+\mu^-$ Collider: A Feasibility Study." *Proceedings of the Snowmass96 Workshop*.

Panofsky, W. K. H. 1997. "The Evolution of Particle Accelerators & Colliders." *Beam Line* 27:36-44.

Roberts, T. 2011. "G4beamline User's Guide 2.08." Batavia, IL.

Shieldwerx.com. 2007. "SWX-201HD 5% Borated Polyethylene." Rio Rancho, NM.

Shieldwerx.com. 2007. "SWX-210 30% Borated Polyethylene." Rio Rancho, NM.

Shieldwerx.com. 2008. "SWX-210 (30% Boron-Poly) Properties and Radiation Thickness Calculator." Rio Rancho, NM.

Skrinsky, A. N. 1980. "Accelerator and Instrumentation Prospects of Elementary Particle Physics." *AIP Conference Proceedings* 68:1056-1093.

Tsai, Y.-S. 1974. "Pair production and bremsstrahlung of charged leptons." *Review of Modern Physics* 46:815-851.

Wikipedia. 2006. Retrieved from http://en.wikipedia.org/wiki/File:Standard_Model_of_Elementary_Particles.svg.

Wright, D. H., Koi, T., Folger, G., Ivantchenko, V., Kossov, M., Starkov, N., Heikkinen, A., Wellisch, H.-P. 2006. *Proceedings of the 12th International Conference on Calorimetry in High Energy Physics (CALOR 06).*

Wu, C. S., Hughes, V. W. 1977. "Introduction and History" in *Muon Physics I: Electromagnetic Interactions* (eds. Hughes, V. W., Wu, C.S.). Academic Press, New York, NY.

Wuest, C. G. 1992. "TART Calculations of Neutron Attenuation and Neutron-induced Photons on 5% and 20% Borated Polyethylene Slabs." *GEM TN-92-172*. Livermore, CA.

Ziemann, V. 2008. "CLIC Post-collision Diagnostics." *EUROTeV-Report-2008-016*.

APPENDIX A:

PARTICLE PROPERTIES

Table 1: Quark Properties

Name	Symbol	Mass	Charge
Up	u	$2.49^{+0.81}_{-0.79}\ \frac{MeV}{c^2}$	$+\frac{2}{3}$
Down	d	$5.05^{+0.75}_{-0.95}\ \frac{MeV}{c^2}$	$-\frac{1}{3}$
Charm	c	$1.27^{+0.07}_{-0.09}\ \frac{GeV}{c^2}$	$+\frac{2}{3}$
Strange	s	$101^{+29}_{-21}\ \frac{MeV}{c^2}$	$-\frac{1}{3}$
Top	t	$172.0 \pm 0.9 \pm 1.3\ \frac{GeV}{c^2}$	$-\frac{1}{3}$
Bottom	b	$4.19^{+0.18}_{-0.06}\ \frac{GeV}{c^2}$	$+\frac{2}{3}$

Table 2: Charged Lepton Properties

Name	Symbol	Mass $\left(\frac{MeV}{c^2}\right)$	Lifetime
Electron	e, e^-	$0.510998910 \pm 0.000000013$	Stable $(> 6 \times 10^{24} yr)$
Muon	μ, μ^-	105.658367 ± 0.000004	$2.197034 \pm 0.000021\ \mu s$
Tau	τ, τ^-	1776.82 ± 0.16	$290.6 \pm 1.0\ fs$

Table 3: Hadron Properties

Name	Symbol	Quark Composition	Mass $\left(\frac{MeV}{c^2}\right)$	Charge	Lifetime
Proton	p, p^+	uud	938.272013 ± 0.000023	$+1$	Stable $(> 2.1 \times 10^{29} yr)$
Neutron	$n. n^0$	udd	939.565346 ± 0.000023	0	$885.7 \pm 0.8\ s$

APPENDIX B:
ELEMENTAL AND CHEMICAL PROPERTIES

Table 4: Table of Selected Elemental Properties

	Boron	Iron	Tungsten
Symbol	$B,\ {}_5B$	$Fe,\ {}_{26}Fe$	$W,\ {}_{74}W$
Atomic Number (Z)	5	26	74
Atomic Weight	10.811	55.845	183.84
Density $\left(\frac{g}{cm^3}\right)$	2.37	7.87	19.3
Nuclear Interaction Length (cm)	35.16	16.77	9.946
Radiation Length (cm)	22.23	1.757	0.3504

Table 5: Table of Boron Isotopes

	Boron-10	Boron-11
Symbol	${}^{10}B$	${}^{11}B$
Abundance	19.9%	80.1%
Isotopic Mass	10.0129370	11.0093054

APPENDIX C:
LIST OF ACRONYMS AND ABBREVIATIONS

ANL	Argonne National Laboratory
APS	Advanced Photon Source
BaBar	B and B-bar ($\bar{B}$) experiment
BNL	Brookhaven National Laboratory
BPE	Borated Polyethylene
CERN	Conseil Européen pour la Recherche Nucléaire (European Council for Nuclear Research), now known as “Organisation Européenne pour la Recherche Nucléaire” (European Organization for Nuclear Research)
CLIC	Compact Linear Collider
DOE	Department of Energy
eV	Electron-Volt
Fermilab	Fermi National Accelerator Laboratory
FNAL	Fermi National Accelerator Laboratory
GeV	Giga-electron-volt
GUI	Graphical User Interface
HPRF	High-Pressure Radio Frequency
ILC	International Linear Collider
IP	Interaction Point
IR	Interaction Region
LEP	Large Electron-Positron [Collider]
LHC	Large Hadron Collider
linac	Linear Accelerator
MAP	Muon Accelerator Program
MerIT	Mercury Intense Target
MeV	Mega-electron-volt
NIL	Nuclear Interaction Length

NNDC	National Nuclear Data Center
NSLS	National Synchrotron Light Sources
PDG	Particle Data Group
RF	Radio Frequency
SLAC	Stanford Linear Accelerator Complex
SM	Standard Model
STTR	Small Business Technology Transfer Program
SUSY	Supersymmetry
TeV	Tera-electron-volt
VLHC	Very Large Hadron Collider

APPENDIX D:
BETHE-HEITLER STATISTICS

Table 6: Bethe-Heitler Simulation Statistics for Iron

Incidents	Energy	Pairs Out	σ	Error	σ (Landau)	σ (High-Z correction)	σ (GEANT4)
(Billions)	(GeV)		(μbarns)				
2	10	601	35.39	1.4	75.48	67.93	33.90
2	25	913	53.76	1.8	101.60	91.44	54.51
2	50	1293	76.14	2.1	121.36	109.22	71.86
2	75	1389	81.79	2.2	132.92	119.63	82.43
2	100	1692	99.63	2.4	141.12	127.01	90.04
2	200	1850	108.94	2.5	160.88	144.79	108.57
2	300	2119	124.78	2.7	172.43	155.19	119.40
2	400	2248	132.37	2.8	180.63	162.57	127.03
2	500	2291	134.91	2.8	187.00	168.30	132.88
2	750	2455	144.56	2.9	198.55	178.70	143.33
2	800	2499	147.15	2.9	200.39	180.35	144.96
2	900	2487	146.45	2.9	203.75	183.38	147.92
2	1000	2522	148.51	3.0	206.75	186.08	150.54
2	2000	2936	172.89	3.2	226.51	203.86	166.91
2	3000	2939	173.06	3.2	238.07	214.26	175.63
2	4000	3126	184.08	3.3	246.27	221.64	181.32
2	5000	3065	180.48	3.3	252.63	227.37	185.43
2	10000	3339	196.62	3.4	272.39	245.15	196.28

Table 7: Bethe-Heitler Simulation Statistics for Tungsten

Incidents	Energy	Pairs Out	σ	Error	σ (Landau)	σ (High-Z correction)	σ (GEANT4)
(Billions)	(GeV)		(μbarns)				
1	10	117	185.54	17.2	611.45	550.31	276.71
1	25	242	383.77	24.7	823.03	740.73	443.48
1	50	367	582.00	30.4	983.09	884.78	583.28
1	75	441	699.35	33.3	1076.71	969.04	668.18
1	100	445	705.70	33.5	1143.14	1028.83	729.22
1	200	560	888.07	37.5	1303.19	1172.88	877.35
1	300	558	884.90	37.5	1396.82	1257.14	963.53
1	400	551	873.80	37.2	1463.25	1316.92	1023.93
1	500	649	1029.21	40.4	1514.77	1363.30	1070.12
1	750	687	1089.47	41.6	1608.40	1447.56	1152.00
1	800	668	1059.34	41.0	1623.30	1460.97	1164.73
1	900	681	1079.95	41.4	1650.50	1485.45	1187.72
1	1000	707	1121.19	42.2	1674.83	1507.35	1208.00
1	2000	823	1305.14	45.5	1834.88	1651.39	1333.06
1	3000	771	1222.68	44.0	1928.51	1735.66	1397.91
1	4000	871	1381.26	46.8	1994.94	1795.44	1439.48
1	5000	870	1379.68	46.8	2046.46	1841.81	1468.97
1	10000	924	1465.31	48.2	2206.51	1985.86	1544.69